UNIVERSIDAD NACIONAL DE COLOMBIA

EEG-based Neuroimaging using Data-Driven Spatio-Temporal Constraints for Non Stationary Brain Activity Reconstruction

Reconstrucción de Actividad Cerebral No-Estacionaria basada en EEG usando Restricciones Espacio-Temporales

Juan Sebastián Castaño Candamil

Universidad Nacional de Colombia
Faculty of Arquitecture and Engineering
Department of Electrical, Electronics and Computer Engineering
Manizales, Colombia
2014

EEG-based Neuroimaging using Data-Driven Spatio-Temporal Constraints for Non Stationary Brain Activity Reconstruction

Reconstrucción de Actividad Cerebral No-Estacionaria basada en EEG usando Restricciones Espacio-Temporales

Juan Sebastián Castaño Candamil

Thesis presented as partial requeriment to obtain the degree::
Master of Engineering

Advisor:
César Germán Castellanos Domínguez, PhD.

Research line:
Industrial Automation
Research Group:
Signal Processing and Recognition Group

Faculty of Arquitecture and Engineering
Department of Electrical, Electronics and Computer Engineering
Manizales, Colombia
2014

Acknowledgements

It is impossible to name every person that one way or another helped me to get here. My sincere apologizes in advance for those who I fail to mention.
Special thanks to Germán Castellanos, my advisor, always willing to support me and discuss the ideas we had. Also to the Signal Processing and Recognition Group, the people from "El Mezzanine", amazingly skilled people, always eager to help you with a math question or just to make a boring afternoon fade away. Juan David Martinez for always listening to anything I wanted to say or discuss. I am also really thankful to the Machine Learning/Neurotechnology group at the Technische Universität Berlin, especially Stefan Haufe and Johannes Höhne. It is almost unbelievable how much I learned in such a short period of time. They also kindly provided the ERP data used in the present work.
Molina and César for discussing life with me, and Juana for sharing it :).
Finally, thanks to my family...

Juan Sebastián

This research was carried out under the projects:

- 111045426008 "Desarrollo de un sistema automático de mapeo cerebral y monitoreo intraoperatorio cortical y profundo: Aplicación a la neurocirugía", funded by COLCIENCIAS.
- 20501007502 "Grupo de Control y Procesamiento Digital de Señales", funded by Universidad Nacional de Colombia.

It was also supported by the scholarship 'Beca de estudiante sobresaliente de posgrado' funded by Universidad Nacional de Colombia.

Abstract

Electroencephalogram(EEG)-based neuroimaging is a widely used technique that allows to non invasively explore brain activity. One of the most prominent advantages of using EEG measures to analyze brain activity is its low cost and outstanding temporal resolution. However, spatial measurement points (electrodes) are relatively low -a couple hundreds in the best case-, while the discretized brain activity generators -termed current dipoles or sources- are several thousands. This leads to a heavily ill-posed mathematical problem commonly known as the EEG inverse problem. To solve such problems, additional information must be a-priori assumed in order to obtain an unique and optimal solution. In the present work, several approaches to improve the accuracy and interpretability of the inverse problem solution are proposed, using physiologically motivated assumptions. Firstly, a method including a realistic time varying autoregressive model is proposed, aiming to explicitly constraining temporal evolution of brain activity. Secondly, another methodology is proposed to relax the brain activity stationarity assumption that is usually made in state-of-art algorithms, this is done by assuming a physiologically motivated time-varying a-priori covariance matrix. Finally, a novel method constraining the solution to a sparse representation in the space-time-frequency domain is introduced. The proposed methods are compared with classic and state-of-art techniques in a simulated environment, and afterwards, are validated using real world data. In general, the contributed approaches are efficient and competitive compared to state-of-art brain mapping methods. **Keywords: EEG, inverse problem, brain mapping**.

Resumen

El mapeo cerebral basado en señales de electroencefalografía (EEG), es una técnica muy usada para explorar la actividad cerebral de forma no invasiva. Una de las ventajas que provee la utilización de señales EEG para analizar la actividad cerebral es su bajo costo y su sobresaliente resolución temporal. Sin embargo la cantidad de puntos de medición (electrodos) es extremadamente baja comparada con la cantidad de puntos discretizados dentro del cerebro sobre los cuales se debe realizar la estimación de la actividad. Esto conlleva a un problema mal condicionado comúnmente conocido como el problema inverso de EEG. Para resolver este tipo de problemas, información apriori debe ser supuesta para así obtener una solución única y óptima. En el presente trabajo investigativo, se proponen distintas aproximaciones a la solución del problema con el objetivo de mejorar la precisión e interpretabilidad de las estimaciones de actividad cerebral. En primer lugar se propone un método que incluye un modelo auto-regresivo, no lineal, realista y variante en el tiempo para restringir las dinámicas temporales de la solución a dicho modelo. En segundo lugar, se propone un algoritmo que permite relajar la suposición de estacionariedad que comúnmente se hace en este tipo de problemas, esto se logra a través de la creación de una matriz de covarianza variante en el tiempo que permite adaptarse a los cambios espacio temporales de la dinámica cerebral. Por último se propone un algoritmo en el cual se representa la actividad cerebral a traves de un conjunto de funciones espacio-temporales las cuales son construidas teniendo en cuenta el contexto fisiológico del problema. Los métodos propuestos son comparados tanto con técnicas clásicas como con métodos del estado del arte usando señales simuladas, y finalmente son validados usando datos EEG reales. En general, los métodos propuestos son eficientes y competitivos en comparación a los métodos usados como referencia. **Keywords: EEG, problema inverso, mapeo cerebral**.

Contents

Notation

Variables and Functions

$\boldsymbol{J}$	Brain activity
$\boldsymbol{j}_k$	Brain activity at time instant k
$\widehat{\boldsymbol{J}}$	Estimated b rain activity
$\widehat{\boldsymbol{j}}_k$	Estimated brain activity at time instant k
$\boldsymbol{L}$	Lead field matrix
$\boldsymbol{Y}$	EEG data
$\boldsymbol{y}_k$	EEG data at time instant k
N_d	Number of dipoles
N_c	Number of electrodes
N_t	Number of time samples
$\boldsymbol{\varepsilon}$	EEG measurement noise
$\boldsymbol{\varepsilon}_k$	EEG measurement noise at time instant t
$f_l(\cdot)$	State transition function for a state space model representation of brain activity
$\boldsymbol{Q}$	A priori covariance matrix of brain activity
$\boldsymbol{Q}_\epsilon$	EEG measurement noise covariance matrix
$\boldsymbol{\Delta}$	Spatial Laplacian operator
$\boldsymbol{I}_n$	Identity matrix of size n
$\boldsymbol{\Phi}_s$	Spatial dictionary
$\boldsymbol{\Phi}_t$	Time frequency dictionary
λ	Regularization parameter
λ_s	Spatial regularization parameter
λ_t	Time-frequency regularization parameter
$\boldsymbol{C}_s$	Coefficients of the spatial basis functions
$\boldsymbol{C}_t$	Coefficients of the time-frequency basis functions
$\boldsymbol{C}$	Coefficients of the spatial-time-frequency basis functions

$\boldsymbol{V}$	Eigenvectors of the EEG temporal covariance matrix

Mathematical Operators

$\text{Diag}(\cdot)$	Diagonal matrix constructed with the argument vector
$\text{trace}(\cdot)$	Trace of the argument
$\text{vec}(\cdot)$	Column major vectorization of the argument matrix
$\|\| \cdot \|\|_F$	Frobenius norm
$\|\| \cdot \|\|_p$	ℓ_p norm
$\boldsymbol{\Theta}(\cdot)$	Energy function of the prior distribution of brain activity $\boldsymbol{J}$
$\otimes$	Kronecker product
$d_g\{\boldsymbol{x}, \boldsymbol{y}\}$	Geodesic distance between $\boldsymbol{x}$ and $\boldsymbol{y}$
$\exp\{\cdot\}$	Gaussian function

Abbreviations

EEG	Electroencephalography
MEG	Magnetoencephalography
SNR	Signal to noise ratio
fMRI	functional Magnetic Resonance Imaging
fNIRS	functional Near Infrared Spectroscopy
PET	Position Emission Tomography
ERP	Evoked Potential Responses
MNE	Minimum Norm Estimates
LORETA	Low Resolution Tomography
sLORETA	Standardized LORETA
LCMV	Linearly Constrained Minimum Variance Beamformer
ARD	Automatic Relevance Determination
GS	Greedy Search
MSP	Multiple Sparse Priors
S-FLEX	Sparse Basis Field Expansion
SVD	Singular Value Decomposition

IRA	Iterative Regularization Algorithm
DOBERMAN	Dynamically Constrained Brain Mapping
MAP	Maximum A Posteriori
TF-MxNE	Time Frequency Mixed Norm Estimates
DNF	Dynamic Neural Fields
STOUT	Spatio-TempOral Unifying Tomography
FISTA	Fast Shrinkage Thresholding Algorithm
STFT	Short Time Fourier Transform

1. Preliminaries

1.1. Introduction

The study of the human brain is of great interest because its complete understanding may lead to effective treatment of several brain diseases, and to the full understanding of human cognitive processes [1]. The main goal is to identify areas of the brain related to certain pathologies or cognitive processes (information extraction in the spatial domain) and also to identify dynamics that rule the activation of brain areas, explaining how they relate with each other and how the brain works as a whole.

However, one of the most limiting issues regarding the study of the brain is information sensing and extraction. Several techniques have been developed to non-invasively extract information about brain functions. Some of these techniques are: functional Magnetic Resonance Imaging (fMRI), functional Near-Infrared Spectroscopy (fNIRS), Positron Emission Tomography (PET), among others. Most of these techniques offer a great spatial resolution, allowing to precisely identify active areas related to certain brain states [30]. Nevertheless, such methods are expensive and, typically, do not offer good temporal resolution, which hinders analysis of brain dynamics and derived physiological interpretations.

On the other hand, Magnetoencephalography (MEG) and Electroencephalography (EEG) are methods that can also be used to study the brain. These techniques are well known for their high temporal resolution [19]. Between MEG and EEG, the latter is more widely used due to its considerably lower cost compared to all the aforementioned methods. EEG analysis have been mainly used to study brain dynamics by identifying and analyzing neural rhythms, Evoked Potential Responses (ERP), epileptic spikes, among others. Nevertheless, EEG recordings also have spatial information because they are usually measured over the entire head surface, and consequently, has also been used as neuroimaging technique. However, the measurement points are relatively low -a couple hundreds at best-, while the discretized brain activity generators -current dipoles or sources- are several thousands. This leads to a heavily ill-posed mathematical problem because the available information is much lower than the information to be inferred [12]. This problem is typically known as the EEG inverse problem or EEG-based neuroimaging.

To solve such problem, additional information must be a-priori assumed in order to get an unique and optimal solution [12]. Classic approaches such as Minimum Norm Estimates (MNE) and LOw REsolution TomogrAphy (LORETA) [22] encourage the simplest (MNE) and/or spatially smoothest (LORETA) solutions. However, these assumptions barely contain specific information about the problem at hand, not to mention information that could be potentially extracted from available EEG recordings. In this regard, sLORETA [21] uses an initial estimation to obtain an smoother, more focal reconstruction in a second estimation stage; another example is the

use of a Linearly-Constrained Minimum Variance (LCMV) beamformer [32] to map sensor-level information to the source level, and then use estimated information to improve the solution [15].

In a probabilistic context, all the methods mentioned above include the a priori information in the form of covariance matrices. Consequently, such methods have been generalized under a framework the defines a set of a-priori covariance matrices -termed priors hereafter-, and then, from this extended and potentially redundant set, the most relevant components are selected, linearly combined and further included in a final estimation stage. This is the main idea behind three iterative Bayesian schemes called Greedy Search (GS), Automatic Relevance Determination (ARD), and Multiple Sparse Priors (MSP) [9]. This approach has been further modified in the Sparse Basis Field Expansion (S-FLEX) algorithm [14] to include the aforementioned spatial constraints in a single-step optimization task. In S-FLEX -as in GS, ARD and MSP-, the prior set corresponds to a dictionary of locally smooth spatial basis functions representing potentially active areas of the brain. The representation of brain activity through such basis functions allows to obtain a spatially coherent solution (solutions that are sparse and locally smooth in the spatial domain).

On the other hand, prior information can also be included in the form of temporal constraints describing the temporal dynamics of neural activity. In this regard, from a general point of view, two approaches have been presented: The first one deals with the inclusion of autoregressive (AR) models to explicitly constraint estimated brain activity time series. The most naive approach -it can be seen as the time-domain equivalent of LORETA- is to model brain activity through a random walk model [27, 28], thereby, encouraging the smoothest time series. A more elaborate approach was introduced in [10] and further analyzed in [3], here, a second order linear model explicitly holding temporal resonance is used. In contrast, the second approach to include a-priori information in the time domain is to automatically identify the main dynamics of available data and use such components as implicit constraints. For example, in [24,25] the temporal components are identified through a SVD decomposition of the temporal covariance matrix of the data and the solution is found using only the most relevant time-domain components. Furthermore, it has been shown that time-frequency representations provide insightful information about dynamics of neural processes. Consequently, using main features of time-frequency representations may significantly improve the solution. Examples of the latter approach can be found in [7, 11, 20, 31].

The present research work is outlined as follows: The remaining pages of the current chapter deal with the mathematical description of classic and state of the art brain mapping methods. Also, the general and specific objectives of the present work are stated. Furthermore, in chapter 2 we discuss the first proposed method, which is an Iterative Regularization algorithm -termed IRA- that allows to include time-varying linear and non linear AR models as time-domain prior information aiming to explicitly describe the dynamics ruling neural activity. Additionally, we present the experimental setup used to simulate the EEG recordings used throughout the manuscript to assess and compare the performance of considered methods. Also, we compare the effects of explicit versus implicit inclusion of temporal information in the EEG inverse solution framework. Moreover, in chapter 3, we describe a novel methodology to include time-varying a-priori information into a standard Bayesian estimation framework. This approach -termed DOBERMAN- allows to relax the assumption of brain activity stationarity while using physiologically motivated spatial a priori information. Finally, in chapter 4, we present a new method that allows to recon-

struct non-stationary activity from space-time-frequency dictionaries using an objective function that encourages spatial coherence and sparsity in the time-frequency domain, thus, representing physiologically plausible assumptions about neural activity.

1.2. Objectives

Based on the aforementioned techniques and their corresponding open issues, we develop the current research work around one general objective which is further expanded into three specific objectives, as follows:

1.2.1. General Objective

To develop a framework that improves the accuracy and interpretability of the EEG inverse problem solution by using physiologically motivated constraints. Such physiologically motivated constraints should be related with the complex spatio-temporal dynamics inherent to the studied problem.

1.2.2. Specific Objectives

- To develop a method that includes a non-linear time varying model to explicitly constrain the time series of the inverse problem solution. The time varying model corresponds to a state of the art model used to describe realistic time series of cortico-thalamic activity.
- To propose a methodology that provides a time varying a priori covariance matrix, aiming to dynamically constrain the spatial distribution of the brain mapping solution, relaxing the stationarity assumption usually found in state of the art methods. To this end a reduced dictionary of spatial basis functions is used to describe brain areas potentially related to different mental states.
- To develop a brain mapping method that provides a solution encoded in a joint space-time-frequency domain through a predefined sparse set of spatial and time-frequency basis functions. To this end, we use the formulation of two state of the art methods and then perform the joint estimation of the weighting coefficients of the spatial and time-frequency basis functions.

1.3. EEG forward and inverse problem formulation

To represent the electromagnetic field measured by EEG, We assume the following linear model [1, 12]:

$$\boldsymbol{Y} = \boldsymbol{L}\boldsymbol{J} + \boldsymbol{\epsilon}, \tag{1-1}$$

where $\boldsymbol{Y} \subset \mathbb{R}^{N_c \times N_t}$ is the EEG data measured by N_c sensors at N_t time samples, $\boldsymbol{J} \subset \mathbb{R}^{3N_d \times N_t}$ is the activity of N_d current dipoles uniformly distributed on the cortical surface with unconstrained

orientation, and $\boldsymbol{L} \subset \mathbb{R}^{N_c \times 3N_d}$ (termed *lead field matrix*) is a gain matrix representing the relationship between current dipoles and EEG data. Also, we assume that $\boldsymbol{Y}$ is affected by a zero mean Gaussian noise $\boldsymbol{\epsilon} \subset \mathbb{R}^{N_c \times N_t}$ with covariance $\text{cov}(\boldsymbol{\epsilon}) = \boldsymbol{Q}_\epsilon = \boldsymbol{I}_{Nc} \subset \mathbb{R}^{N_c \times N_c}$, where $\boldsymbol{I}$ is an identity matrix.

Within a Bayesian framework, the EEG inverse problem may be formulated as a Maximum A Posteriori -MAP- estimation procedure by finding the most probable estimation $\widehat{\boldsymbol{J}}$ with regards to measured EEG data and a priori considerations, that is, as the argument maximizing the following posterior estimation problem: $\underset{\boldsymbol{J}}{\text{argmax}} \left\{ p\left(\boldsymbol{Y}|\boldsymbol{J}\right) p\left(\boldsymbol{J}\right) \right\}$, where $p(\boldsymbol{Y}|\boldsymbol{J})$ is the conditional posterior probability of $\boldsymbol{J}$ given the measurements $\boldsymbol{Y}$ and $p(\boldsymbol{J})$ is the prior distribution of $\boldsymbol{J}$. Moreover, assuming the posterior density to have a Gaussian distribution, the estimation of $\boldsymbol{J}$ leads to the following minimization problem [12]:

$$\underset{\boldsymbol{J}}{\text{argmin}} \{ ||\boldsymbol{Y} - \boldsymbol{L}\boldsymbol{J}||_F^2 + \lambda \Theta\left(\boldsymbol{J}\right) \} \tag{1-2}$$

where $\| \cdot \|_F$ denotes the Frobenius-norm, $\lambda \subset \mathbb{R}^+$ is a tuning or regularization parameter, and $\Theta\left(\boldsymbol{J}\right) \subset \mathbb{R}^+$ is an energy function associated with $p(\boldsymbol{J})$ and corresponds to the so called prior.

1.4. Selection of prior information in the spatial domain

If the prior is assumed to be Gaussian, i.e., when $\Theta\left(\boldsymbol{J}\right)$ represents a Gaussian distribution with zero mean and covariance matrix $\boldsymbol{Q}$; estimation of brain activity $\widehat{\boldsymbol{J}}$ can be computed as function $f(\boldsymbol{Q}, \boldsymbol{Y})$: $\widehat{\boldsymbol{J}} = \boldsymbol{Q}\boldsymbol{L}^\top (\boldsymbol{Q}_\epsilon + \boldsymbol{L}\boldsymbol{Q}\boldsymbol{L}^\top)^{-1}\boldsymbol{Y}$. Since prior $\boldsymbol{Q}$ is a parameter that heavily affects the solution, its selection is an issue of great interest.

Non-informed approaches Particularly, the simplest approach for selecting $\boldsymbol{Q}$ is to define it as $\boldsymbol{Q} = \boldsymbol{I}_{3N_d}$, which corresponds to MNE [23]. A more elaborated approach -LORETA [22]- defines $\boldsymbol{Q}{=}(\boldsymbol{\Delta}^\mathsf{T}\boldsymbol{\Delta})^{-1}$, being $\boldsymbol{\Delta} \subset \mathbb{R}^{3N_d \times 3N_d}$ the spatial Laplacian operator, which encourages smoothness in the spatial domain. Yet, both plain estimators do not reflect significant physiological properties of the problem at hand and consequently are termed non-informed approaches.

Informed approaches Instead, there are also the informed estimators, that explicitly extract information provided by available EEG signals. For example, sLORETA [21] and Linear Constrained Minimum Variance Beamformer (LCMV) [15] perform a two stage estimation process in which the second estimation is computed using a covariance matrix calculated in the first stage using available EEG measurements.

Multiple Sparse Priors (MSP)

To make more flexible the definition of $\boldsymbol{Q}$, both informed and non-informed estimation approaches can be gathered under a generalized framework, as discussed in [9, 33], where the matrix $\boldsymbol{Q}$ is expressed in terms of a linear combination of a fixed, but known set of components contained in

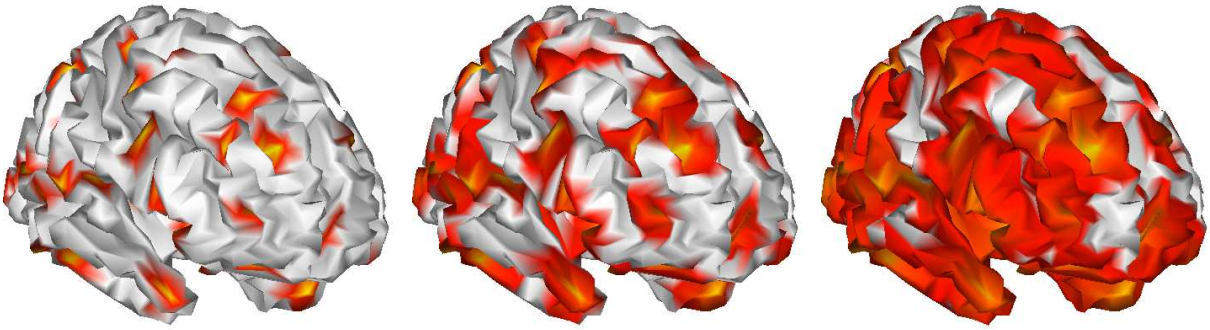

(a) Small (b) Medium (c) Large

Figure **1-1**.: Example of spatial patches, with different sizes, used in ARD/GS/MSP and S-FLEX. Each column of $\boldsymbol{\Phi}_s$ corresponds to a single cortical patch.

the columns of a given matrix $\boldsymbol{\Phi}_s \subset \mathbb{R}^{3N_d \times N_s}$ as follows:

$$\boldsymbol{Q} = \sum_{i \in N_s} h_i \, \mathrm{Diag}\left(\boldsymbol{\Phi}_s(\cdot, i)\right) \tag{1-3}$$

where $\mathrm{Diag}\left(\boldsymbol{\Phi}_s(\cdot, i)\right) \subset \mathbb{R}^{3N_d \times 3N_d}$ is a diagonal matrix formed by the ith column of $\boldsymbol{\Phi}_s$ and holding a given prior component; $h_i \subset \mathbb{R}$ is a weighting hyperparameter, which is commonly calculated based on the EEG data covariance [33].

Given that brain activity is expected to happen in sparse and locally smooth brain areas (referred as spatial coherence), the set $\boldsymbol{\Phi}_s$ can be extended by defining each column of $\boldsymbol{\Phi}_s$ as a potentially active cortex area (termed cortical or spatial patch), as illustrated in Figure **1-1**.

The use of an extended set $\boldsymbol{\Phi}_s$ that is formed by a set of cortical patches is the main idea behind Automatic Relevance Determination (ARD), Greedy Search (GS), and by extension the Multiple Sparse Priors (MSP), presented in [9] and explored to a greater extent in [5, 33]. In all of these algorithms, the estimation problem is further constrained by assuming that a small set of spatial patches is enough to explain observed data, i.e., there is an sparsity assumption in the estimation of the coefficient set $\{h_i\}$ which is achieved by assuming that such parameters follow the Laplacian distribution.

Sparse Basis Field Expansion (S-FLEX)

Furthermore, spatial sparsity can also be formulated within a single step optimization task. For example, prior information of $\boldsymbol{J}$ can be assumed to behave according to the Laplace distribution with zero mean and identity matrix covariance. This assumption is equivalent to fix $\Theta\left(\boldsymbol{J}\right) = ||\boldsymbol{J}||_1$, where $||\cdot||_1$ is the ℓ_1-norm. Consequently, the optimization problem in Eq. (1-2) is redefined as (a.k.a. the LASSO problem [29]):

$$\underset{\boldsymbol{J}}{\mathrm{argmin}}\{||\boldsymbol{Y} - \boldsymbol{L}\boldsymbol{J}||_F^2 + \lambda||\boldsymbol{J}||_1\} \tag{1-4}$$

However, formulation in Eq. (1-4) usually leads to unstable and scattered active sources that may not be physiologically plausible, as discussed in [12, 14]. To address this issue, the Sparse Basis Field Expansion (S-FLEX) algorithm is developed in [14], where current dipoles are redefined as a linear combination of locally smooth spatial basis functions spread over the brain:

$$\boldsymbol{J} = \boldsymbol{\Phi}_s \boldsymbol{C}_s \tag{1-5}$$

where matrix $\boldsymbol{C}_s \subset \mathbb{R}^{N_s \times N_t}$ contains the weighting coefficients that are assumed to have a Laplacian prior distribution. According to the aforementioned representation, and to obtain spatially sparse solutions, the following objective function is derived:

$$\arg\min_{\boldsymbol{C}_s} \{||\boldsymbol{Y} - \boldsymbol{L}\boldsymbol{\Phi}_s \boldsymbol{C}_s||_F^2 + \lambda ||\boldsymbol{C}_s||_{1,2}\} \tag{1-6}$$

where the notation $||\cdot||_{1,2}$ stands for the $\ell_{1,2}$-norm that is the ℓ_1-norm grouping each vector dipole component under the ℓ_2-norm to avoid orientation bias [14].
Once the matrix $\boldsymbol{C}_s$ has been estimated, then neural activity is recovered by using Eq. (1-5). Furthermore, temporal inconsistencies produced by instantaneous S-FLEX solution that assumes EEG observations as independent at each time sample, temporal coherence (smooth time series) may be improved by accepting activation of the same brain areas during the entire EEG segment. Bearing this in mind, Eq. (1-6) is rewritten to group each dipole time series under the $\ell_{1,2}$-norm, considering that brain activity remains stationary for the whole analyzed time window, as usually assumed by brain mapping methods [11, 12]. However, it is commonly accepted that brain activity has non–stationary nature. Therefore, stationarity assumption may hinder brain mapping accuracy

1.5. Selection of prior information in the time domain

In general, the use of the MAP estimator -in the way we have studied it so far- allows to obtain an static solution, i.e., each time sample is treated as an *independent* solution, thus it does not include temporal dynamics that an EEG recording could offer to improve brain mapping accuracy. In this regard, time domain information can be included explicitly or implicitly, depending on whether an explicit dynamical model is used to describe time-domain properties of neural activity, or on the contrary, a set of automatically identified dynamics are used to constraint the solution. In the remainder of this section We will explore both approaches.

1.5.1. State space modeling

The formulation of the model written in Eq. (1-1) can be augmented to a state space model to explicitly constrain the temporal evolution of the neuronal activity through a predefined state transition model, as follows

$$\boldsymbol{j}_k = f_l(\boldsymbol{j}_{k-1}, \ldots, \boldsymbol{j}_{k-n}, \boldsymbol{w}) + \boldsymbol{\eta}_k, \tag{1-7a}$$

$$\boldsymbol{y}_k = \boldsymbol{L}\boldsymbol{j}_k + \boldsymbol{\epsilon}_k, \tag{1-7b}$$

where $\boldsymbol{\eta}_k \subset \mathbb{R}^{N_d \times 1}$ is the normally distributed process noise, i.e., $\boldsymbol{\eta}_k \sim \mathcal{N}(\boldsymbol{0}, \boldsymbol{Q})$, $\boldsymbol{w} \in \mathbb{R}^{N_p \times 1}$ holds N_p parameters of function f_l, and $\boldsymbol{j}_k \in \mathbb{R}^{N_d \times 1}$ and $\boldsymbol{y}_k \in \mathbb{R}^{N_c \times 1}$ are vectors containing brain activity

and EEG measurements at time instant k, respectively.
Early approaches define state transition model f_l as a random walk model [27, 28] -encouraging smoothness in the temporal domain-, e.g., $\boldsymbol{j}_k = \boldsymbol{I}_{3N_d}\boldsymbol{j}_{k-1}$, where $\boldsymbol{I}_{3N_d} \subset \mathbb{R}^{3N_d \times 3N_d}$. More recent approaches describe the temporal evolution of neural activity as a second order linear model that allows to describe brain activity resonance [3,10]: $\boldsymbol{j}_k = (a_1\boldsymbol{I}_{N_d}+b_1\boldsymbol{\Delta})\boldsymbol{j}_{k-1}+a_2\boldsymbol{I}_{N_d}\boldsymbol{j}_{k-2}$. In either way the task remains as the estimation of hidden states $\boldsymbol{j}_k$ which can be carried out using for example, the Kalman filter. However, it has been suggested that such approaches are too simple to describe the complex dynamics that brain activity can present during different mental states [3, 34].

1.5.2. Data driven temporal components identification

Given the complexity of brain activity dynamics, we are also interested in exploring how main temporal features of available EEG measures can be used to implicitly constrain time-domain components found in the brain activity estimation.

Main temporal components

In [24, 25], the authors propose that the temporal information contained in $\widehat{\boldsymbol{J}}$ corresponds only to the first N_q main temporal components of available data $\boldsymbol{Y}$. This is achieved by projecting input data $\boldsymbol{Y}$ into the first N_q eigenvectors of the temporal covariance matrix that is obtained from the SVD decomposition $\boldsymbol{V}\boldsymbol{S}\boldsymbol{V}^\mathsf{T}=\boldsymbol{Y}^\mathsf{T}\boldsymbol{Y}$, where $\boldsymbol{V} \subset \mathbb{R}^{N_t \times N_t}$ is a matrix where each column corresponds to the right singular vectors (temporal components) of $\boldsymbol{Y}$, and $\boldsymbol{S} \subset \mathbb{R}^{N_t \times N_t}$ is a matrix holding the corresponding eigenvalues in the main diagonal. Then, the solution is calculated using as observation set the projection $\boldsymbol{Y}\boldsymbol{V}$. Then, the resulting estimation is projected back to the original space, i.e., $\widehat{\boldsymbol{J}} = \widehat{\boldsymbol{J}}_p\boldsymbol{V}^\mathsf{T}$, where $\widehat{\boldsymbol{J}}_p$ is the estimated activity in the projected space.

Time-frequency representation

Since brain activity should be assumed as non-stationary, time–frequency representations of neural activity has been proposed before to investigate dynamic properties of the EEG data during transient physiological episodes. For example in [7, 20], raw data is represented with a set of time-frequency atoms, and then the estimation is carried out using such representation as available observations. Consequently, brain activity reconstruction is constrained to a set of time-frequency atoms selected according to the information contained in available EEG data.

Time-Frequency Mixed Norms Estimate The aforementioned time-frequency approaches may be modified to include time-domain constraints not at the sensor level -as described so far-, but instead, directly at the source level. To address this issue, Time Frequency Mixed Norm Estimates (TF-MxNE) algorithm is presented in [11]. Here, time-frequency domain priors are considered using several predefined time-frequency atoms encoding non-stationary dynamics. Thus, brain activity $\boldsymbol{J}$ is now redefined in terms of a predefined time-frequency dictionary:

$$\boldsymbol{J}=\boldsymbol{C}_t\boldsymbol{\Phi}_t, \tag{1-8}$$

where $\boldsymbol{\Phi}_t \subset \mathbb{C}^{N_f \times N_t}$ holds a set of N_f time-frequency basis functions, and $\boldsymbol{C}_t \subset \mathbb{C}^{N_d \times N_f}$ is the coefficient set to be estimated. To maintain the sparse row structure in the coefficients (to guarantee that only a few sources are active during the entire analysis interval), while simultaneously promoting sparsity of the time-frequency decompositions (only a few basis functions are used to explain brain activity), the following composite prior formed by the sum of $\ell_{1,2}$ and ℓ_1-norms is used: $\Theta\left(\boldsymbol{C}_t\right) = \lambda_s \|\boldsymbol{C}_t\|_{1,2} + \lambda_t \|\boldsymbol{C}_t\|_1$, where $\lambda_s \subset \mathbb{R}^+$ and $\lambda_t \subset \mathbb{R}^+$ are the regularization parameters ruling spatial and temporal sparsity, respectively. Consequently, the objective function in Eq. (1-2) is modified to include the aforementioned priors as follows [11]:

$$\arg\min_{\boldsymbol{C}_t} \{||\boldsymbol{Y} - \boldsymbol{L}\boldsymbol{C}_t\boldsymbol{\Phi}_t||_F^2 + \lambda_s||\boldsymbol{C}_t||_{1,2} + \lambda_t||\boldsymbol{C}_t||_1\} \tag{1-9}$$

Although, time-frequency sparsity provides robustness to noise because low energy atoms (commonly related to noise) are trimmed to zero, placing in Eq. (1-9) the $\ell_{1,2}$-norm prior directly on the dipoles may lead to scattered and spatially unstable solutions that are inherent to the ℓ_1-norm estimator.

2. Time-varying state space models in an iterative regularization framework - IRA

2.1. Introduction

To improve brain mapping accuracy, spatial and temporal dynamics inherent to neural processes should be considered within the inverse problem solution framework [26]. Specifically, temporal dynamics can be included in the form of a dynamic estimation model that constrains the solution to some predefined geometric or physiological restrictions. Particularly in [27,28], the time domain of the solution is constrained to a temporal random walk model, i.e., maximum temporal smoothness, however, this model is not physiologically meaningful. Since a physiologically motivated model would allow an adequate description of the system dynamics, it increases information provided by the inverse solution. To this end, an improvement in the description of the source dynamics is accomplished grounded on the telegrapher's equation, explicitly holding temporal resonance, as proposed in [2,10]. Under this framework, however, the dynamic estimation model is restricted to be linear. Instead, we propose the use of Dynamic Neural Fields (DNF) approximating non-linear dynamic models, which may improve brain mapping accuracy since these non-linear models are more realistic and allow a better representation of neural dynamics [6, 17, 18]. In this chapter, we propose the estimation of brain activity using a state space model that includes time-varying DNF-models to describe brain activity. Under this framework, the time-varying parameters of the DNF-model are calculated iteratively at each time sample without significantly increasing the computational burden. The proposed method is validated using real EEG data containing ictal and interictal events for four different epilepsy patients.

2.2. Materials and Methods

2.2.1. Brain Activity Description using Autoregressive Models

We will consider dynamic systems described by the following equation system:

$$\boldsymbol{w}_k = g\left(\boldsymbol{w}_{k-1}\right) + \boldsymbol{\epsilon}_k \tag{2-1a}$$

$$\boldsymbol{j}_k = f_l\left(\boldsymbol{j}_{k-1}, \ldots, \boldsymbol{j}_{k-m}, \boldsymbol{w}_k\right) + \boldsymbol{\eta}_k \tag{2-1b}$$

$$\boldsymbol{y}_k = \boldsymbol{L}\boldsymbol{j}_k + \boldsymbol{\varepsilon}_k \tag{2-1c}$$

where g is a linear vectorial function of first order that models the dynamics of $\boldsymbol{w}_k \subset \mathbb{R}^{N_p \times 1}$ (the N_p time varying parameters of function f_l), and $\boldsymbol{\epsilon}_k \in \mathbb{R}^{p \times 1}$ represents the noise in the model of

the N_p time varying parameters. Specifically, Eq. (2-1c) is the discrete time measure, Eq. (2-1b) describes state evolution, and Eq. (2-1a) is the parameter evolution.
In Eq. (2-1b), the current density dynamics can be modeled by using DNF incorporating cortico-thalamic connectivity and thalamic nonlinearity [6, 18]:

$$\left(\frac{1}{\gamma_a^2}\frac{\partial^2}{\partial t^2}+\frac{2}{\gamma_a}\frac{\partial}{\partial t}+1-r_a^2\nabla^2\right)\boldsymbol{j}\left(\boldsymbol{r},t\right)=\boldsymbol{q}\left(\boldsymbol{\rho}\right) \tag{2-2}$$

where $\gamma_a \in \mathbb{R}$ is the mean decay rate, $r_a \in \mathbb{R}$ is the mean range of axons a, and $\boldsymbol{q}_{(r)} = q_{max}/(1 + \exp((-\boldsymbol{\rho}_{(r)} - \theta)/\sigma))$, with $\boldsymbol{q}_{(r)}$ being the rth element of vector $\boldsymbol{q} \in \mathbb{R}^{3N_d\times 1}$, that is the mean firing rate of excitatory and inhibitory neurons. Vector $\boldsymbol{q}$ is nonlinearly related to mean potentials $\boldsymbol{\rho} \in \mathbb{R}^{3N_d\times 1}$, being $\theta \in \mathbb{R}^+$ the mean firing threshold, $\sigma \in \mathbb{R}^+$ its standard deviation, and $q_{max} \in \mathbb{R}^+$ the maximum firing rate.
Furthermore, the following is a discretized version of the continuous time model in Eq. (2-2) [6]:

$$\boldsymbol{f}\left(\boldsymbol{j}_{k-1},\ldots,\boldsymbol{j}_{k-2}\right)=\boldsymbol{A}_1\boldsymbol{j}_{k-1}+\boldsymbol{A}_2\boldsymbol{j}_{k-1}^2+\boldsymbol{A}_3\boldsymbol{j}_{k-1}^3+\boldsymbol{A}_4\boldsymbol{j}_{k-2}+\boldsymbol{A}_5\boldsymbol{j}_{k-\tau}, \tag{2-3}$$

where $\boldsymbol{A}_1 = a_1\boldsymbol{I}_{3N_d} + b_1\boldsymbol{\Delta}$, $\boldsymbol{A}_2 = a_2\boldsymbol{I}_{3N_d}$, $\boldsymbol{A}_3 = a_3\boldsymbol{I}_{3N_d}$, $\boldsymbol{A}_4 = a_4\boldsymbol{I}_{3N_d}$, and $\boldsymbol{A}_5 = a_5\boldsymbol{I}_{3N_d}$, where $\boldsymbol{\Delta} \in \mathbb{R}^{3N_d\times 3N_d}$ is the spatial Laplacian matrix holding all spatial interactions among sources, and τ is a delayed feedback.

2.2.2. An iterative regularization algorithm

As a concrete solution of the dynamic inverse problem, estimation of both neural activity $\boldsymbol{j}_k$, and discrete non-linear parameters $\boldsymbol{w}_k$, can be formulated from Eqs. (2-1c), (2-1b), and (2-1a) as the following optimization task:

$$\underset{\boldsymbol{j}_k,\boldsymbol{w}_k}{\arg\min}\left\{\left\|\boldsymbol{P}\left(\boldsymbol{y}_k-\boldsymbol{L}\boldsymbol{j}_k\right)\right\|_2^2+\lambda\left\|\boldsymbol{R}\left(\boldsymbol{j}_k-\boldsymbol{f}\left(\widehat{\boldsymbol{j}}_{k-1},\cdots,\widehat{\boldsymbol{j}}_{k-m},\boldsymbol{w}_k\right)\right)\right\|_2^2+\gamma\left\|\boldsymbol{H}\left(\boldsymbol{w}_k-\boldsymbol{g}\left(\widehat{\boldsymbol{w}}_{k-1}\right)\right)\right\|_2^2\right\} \tag{2-4}$$

where the state estimation $\widehat{\boldsymbol{j}}_{k-i}$ is carried out at the $(k-i)$-th step, $\widehat{\boldsymbol{w}}_{k-1}$ is the parameter also estimated at the $(k-1)$-th step, $\lambda \in \mathbb{R}^+$ and $\gamma \in \mathbb{R}^+$ are the regularization parameters ruling minimization of each functional term, and $\boldsymbol{P} \in \mathbb{R}^{N_c\times N_c}$, $\boldsymbol{R} \in \mathbb{R}^{3N_d\times 3N_d}$, and $\boldsymbol{H} \in \mathbb{R}^{p\times p}$ represent weighting matrices that are related to the noise covariance matrices of the measure set $\boldsymbol{y}_k$, state $\boldsymbol{j}_k$, and parameter $\boldsymbol{w}_k$, respectively. Also, the following equivalent representation of the norm $||\cdot||_2^2$ is considered: $\left\|\boldsymbol{P}\left(\boldsymbol{a}-\boldsymbol{b}\right)\right\|_2^2 = \left(\boldsymbol{a}-\boldsymbol{b}\right)^{\mathsf{T}}\boldsymbol{P}^{\mathsf{T}}\boldsymbol{P}\left(\boldsymbol{a}-\boldsymbol{b}\right)$. Consequently, the aforementioned relationship between weighting covariance matrices are redefined in the following form: The covariance matrix of the scalp measures, $\boldsymbol{Q}_\epsilon = \left(\boldsymbol{P}^{\mathsf{T}}\boldsymbol{P}\right)^{-1}$, with $\boldsymbol{Q}_\epsilon \in \mathbb{R}^{N_c\times N_c}$, the state covariance, $\boldsymbol{Q} = \left(\boldsymbol{R}^{\mathsf{T}}\boldsymbol{R}\right)^{-1}/\lambda$, with $\boldsymbol{Q} \in \mathbb{R}^{3N_d\times 3N_d}$, and the parameter noise covariance $\boldsymbol{\Gamma} = \left(\boldsymbol{H}^{\mathsf{T}}\boldsymbol{H}\right)^{-1}/\gamma$, with $\boldsymbol{\Gamma} \in \mathbb{R}^{p\times p}$. So, defining the objective function of Eq. 2-4 as the functional $\Psi\left(\boldsymbol{j}_k,\boldsymbol{w}_k,\lambda,\gamma\right)$, it may be rewritten in the form:

$$\begin{aligned}\Psi\left(\boldsymbol{j}_k,\boldsymbol{w}_k,\boldsymbol{\Lambda},\boldsymbol{\Gamma}\right) = &\left(\boldsymbol{y}_k-\boldsymbol{L}\boldsymbol{j}_k\right)^{\mathsf{T}}\boldsymbol{Q}_\epsilon^{-1}\left(\boldsymbol{y}_k-\boldsymbol{L}\boldsymbol{j}_k\right)\\ &+\left(\boldsymbol{j}_k-\boldsymbol{f}\left(\widehat{\boldsymbol{j}}_{k-1},\ldots,\widehat{\boldsymbol{j}}_{k-m},\boldsymbol{w}_k\right)\right)^{\mathsf{T}}\boldsymbol{Q}^{-1}\left(\boldsymbol{j}_k-\boldsymbol{f}\left(\widehat{\boldsymbol{j}}_{k-1},\ldots,\widehat{\boldsymbol{j}}_{k-m},\boldsymbol{w}_k\right)\right)\\ &+\left(\boldsymbol{w}_k-\boldsymbol{g}\left(\widehat{\boldsymbol{w}}_{k-1}\right)\right)^{\mathsf{T}}\boldsymbol{\Gamma}^{-1}\left(\boldsymbol{w}_k-\boldsymbol{g}\left(\widehat{\boldsymbol{w}}_{k-1}\right)\right)\end{aligned} \tag{2-5}$$

The above multivariate optimization task is solved by iteratively optimizing one variable at a time, while remaining variables are kept fixed. Consequently, given a known state estimation $\widehat{\boldsymbol{j}}_k$, estimation of the model parameters $\widehat{\boldsymbol{w}}_k$ can be obtained by minimizing Eq. (2-5) with respect to $\boldsymbol{w}_k$, that is:

$$\widehat{\boldsymbol{w}}_k = \arg\min_{\boldsymbol{w}_k} \left\{ \Psi \left(\widehat{\boldsymbol{j}}_k, \boldsymbol{w}_k, \boldsymbol{\Lambda}, \boldsymbol{\Gamma} \right) \right\} \tag{2-6}$$

After replacing $\boldsymbol{j}_k$ with $\widehat{\boldsymbol{j}}_k$ in Eq. (2-5), the minimization task in Eq. (2-6) is accomplished by calculating the Jacobian with respect to $\boldsymbol{w}_k$, which is determined as follows:

$$\begin{aligned} \nabla_{\boldsymbol{w}_k} \Phi \left(\widehat{\boldsymbol{j}}_k, \boldsymbol{w}_k, \boldsymbol{Q}, \boldsymbol{\Gamma} \right) =& 2 \left(\boldsymbol{G}_k^{\mathsf{T}} \boldsymbol{Q}^{-1} \boldsymbol{G}_k + \boldsymbol{\Gamma}^{-1} \right) \boldsymbol{w}_k \\ & - 2 \boldsymbol{G}_k^{\mathsf{T}} \boldsymbol{Q}^{-1} \widehat{\boldsymbol{j}}_k - 2 \boldsymbol{\Gamma}^{-1} \boldsymbol{g} \left(\widehat{\boldsymbol{w}}_{k-1} \right) \end{aligned} \tag{2-7}$$

where $\boldsymbol{G}_k = \partial \boldsymbol{f} / \partial \boldsymbol{w}_k$, with $\boldsymbol{G}_k \in \mathbb{R}^{3N_d \times p}$.
Hence, once equaling Eq. (2-7) to $\mathbf{0}$, estimation $\widehat{\boldsymbol{w}}_k$ is reached:

$$\widehat{\boldsymbol{w}}_k = \left(\boldsymbol{G}_k^{\mathsf{T}} \boldsymbol{Q}^{-1} \boldsymbol{G}_k + \boldsymbol{\Gamma}^{-1} \right)^{-1} \left(\boldsymbol{G}_k^{\mathsf{T}} \boldsymbol{Q}^{-1} \widehat{\boldsymbol{j}}_k + \boldsymbol{\Gamma}^{-1} \boldsymbol{g} \left(\widehat{\boldsymbol{w}}_{k-1} \right) \right)$$

Likewise, provided the known parameter set $\widehat{\boldsymbol{w}}_k$, and Jacobian with respect to $\boldsymbol{j}_k$ expressed as:

$$\begin{aligned} \nabla_{\boldsymbol{j}_k} \Phi \left(\boldsymbol{j}_k, \widehat{\boldsymbol{w}}_k, \boldsymbol{Q}, \boldsymbol{\Gamma} \right) =& 2 \left(\boldsymbol{L}^{\mathsf{T}} \boldsymbol{Q}_{\epsilon}^{-1} \boldsymbol{L} + \boldsymbol{Q}^{-1} \right) \boldsymbol{j}_k \\ & - 2 \boldsymbol{L}^{\mathsf{T}} \boldsymbol{Q}^{-1} \boldsymbol{y}_k - 2 \boldsymbol{Q}^{-1} \boldsymbol{f} \left(\widehat{\boldsymbol{j}}_{k-1}, \ldots, \widehat{\boldsymbol{j}}_{k-m}, \widehat{\boldsymbol{w}}_k \right), \end{aligned} \tag{2-8}$$

estimation of the current density vector $\widehat{\boldsymbol{j}}_k$ is also performed by minimizing functional in Eq. (2-5) with respect to $\boldsymbol{j}_k$. So, we get the following estimation $\widehat{\boldsymbol{j}}_k$:

$$\widehat{\boldsymbol{j}}_k = \left(\boldsymbol{I}_{3N_d} - \boldsymbol{Q} \boldsymbol{L}^{\mathsf{T}} \left(\boldsymbol{L} \boldsymbol{Q} \boldsymbol{L}^{\mathsf{T}} + \boldsymbol{Q}_{\boldsymbol{\epsilon}} \right)^{-1} \boldsymbol{L} \right) \left(\boldsymbol{Q} \boldsymbol{L}^{\mathsf{T}} {\boldsymbol{Q}_{\boldsymbol{\epsilon}}}^{-1} \boldsymbol{y}_k + \boldsymbol{f} \left(\widehat{\boldsymbol{j}}_{k-1}, \ldots, \widehat{\boldsymbol{j}}_{k-m}, \widehat{\boldsymbol{w}}_k \right) \right) \tag{2-9}$$

Overall, the dual iterative estimation of $\widehat{\boldsymbol{w}}_k$ and $\widehat{\boldsymbol{j}}_k$ requires only some inverse calculations of sizes $N_p \times N_p$ and $N_c \times N_c$, respectively, making this method suitable for practical implementation.

2.3. Experimental Setup

In the present section we describe the simulations and general setup of the experiments utilized to assess the performance of the analyzed methods throughout the present research work.

2.3.1. Simulated EEG data generation

The most common approach to assess the EEG inverse solution is the use of simulated EEG recordings where brain activity is known, so that estimation quality can be objectively validated. In this work, activity is simulated for one, three, and five active dipoles with random location and orientation. Since in the present work most of real data used to validate the considered methods corresponds to time-locked data (as for example ERP), simulated data sets are generated using the

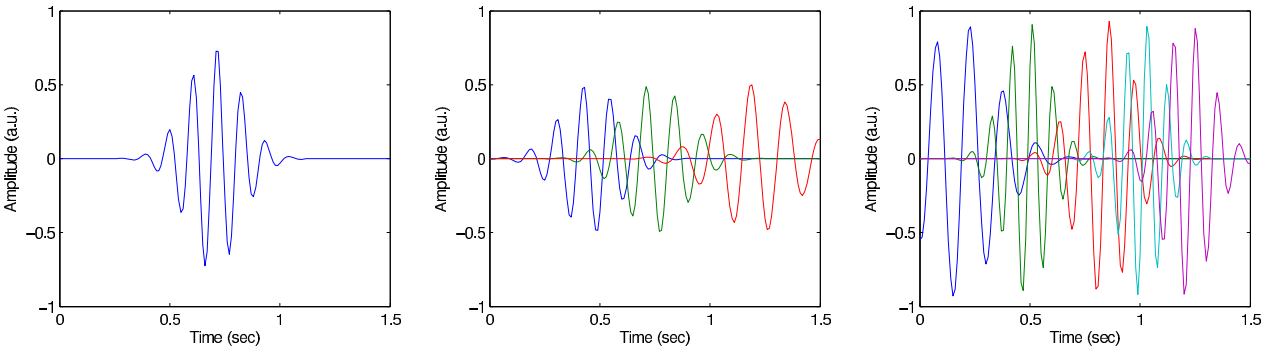

(a) One active source (b) Three active sources (c) Five active sources

Figure **2-1**.: Examples of the time series used in the simulations for different number of active dipoles.

same trial-based model. Figure **2-1** shows examples of generated time series for different number of active dipoles used in the experiments. Similarly to the activity used in the simulations in [11], each time series of the active dipoles is generated using real Morlet wavelets with a length of 1.5 s, sampled at 120 Hz, and holding the following parameters:

- Random central frequency with a mean of 9 Hz and standard deviation of 2 Hz, sampled from a Gaussian distribution.
- Random time shift generated by normal distribution with standard deviation of 0.05 s and mean value that is selected depending on the number of active sources as follows: 0.75 s for one active source; 0.375 s, 0.75 s, and 1.25 s for three active sources; 0.25 s, 0.5 s, 0.75 s, 1 s, and 1.25 s for five active sources.

To get more realistic simulations, we consider both biological and measurement noises for each trial. The former noise stands for neural activity being not related to the ERP under consideration, i.e., background brain activity, whereas the latter component represents together environmental and acquisition noise. As typically assumed for biological systems, we model the biological noise as having the power spectral density inversely proportional to the frequency (also referred to as flicker or pink noise). Specifically, we add pink noise to 1000 randomly selected dipoles for each trial, and the amplitude of these spurious sources is set as $-5\,dB$ Signal-to-Noise Ratio (SNR) at the source level. Therefore, each trial is computed by first multiplying the simulated brain activity with the fixed lead field matrix and then adding measurement noise as to get an SNR of $0\,dB$ at the sensor level. Since ERPs are derived by averaging EEG to time-locked stimulus events, yielding a SNR proportional to the number of averaged trials, we select the number of trials as 5, 20, 50, 100, and 250, to calculate mapping accuracy at the following SNR values: $-5, 0, 7, 12$, and 14 dB, respectively. As a result, 50 runs are carried out to obtain statistically significant results for each combination of number of trials and number of active dipoles.
In turn, the head model used to generate the lead field matrix comprises 4000 dipoles placed only on the tessellated cortex surface. In some studies, dipoles have been assumed to be perpendicular to the cortex surface since main EEG data generators are the pyramidal cortical neurons, whose

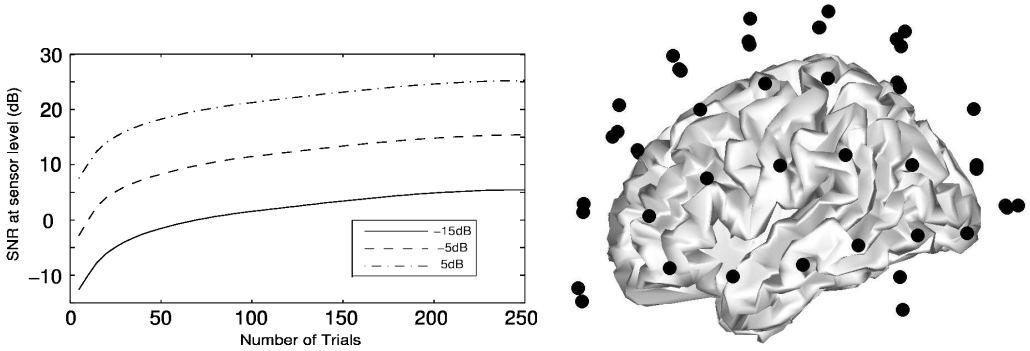

(a) Relation between number of trials and SNR for three different noise levels at source space.

(b) Cortical manifold and electrodes used in the simulations and real data analysis.

Figure **2-2**.: Details of the model used in the simulation of EEG data.

dendritic trunks are locally oriented in parallel and pointing perpendicularly to the cortical surface [1]. However, if a reliable head model of a concrete studied subject is not available (that is, when using atlases), this assumption cannot be trusted. Therefore, given that we use an atlas in the present study, a dipole set with unknown values of amplitude and orientation is considered, yielding a total of 12000 unknowns per time instant: 3 variables per dipole that represent activity strength in each one of the three dimensional directions.
Furthermore, the simulated brain activity is *measured* by 59 electrodes placed according to the international 10-20 system. The visual representation of the cortex and sensor locations can be seen in Figure **2-2**.

2.3.2. Depth bias compensation

Since it is difficult for EEG recordings to detect deep neural generators, the reconstructions are typically biased towards reconstructing superficial sources. Therefore, the so called "depth bias compensation" procedure should be carried out to avoid such bias. In Appendix A, we have studied different methods serving this purpose. Although, throughout the present work we have used the following depth compensation procedure, presented in [11].
Specifically, for the ith column of $\boldsymbol{L}$, i.e., $\boldsymbol{L}(\cdot, i)$, the normalization term is calculated as follows

$$\boldsymbol{\Omega(i,i)} = \sqrt{(||\boldsymbol{L}_x(\cdot,i)||_2^2 + ||\boldsymbol{L}_y(\cdot,i)||_2^2 + ||\boldsymbol{L}_z(\cdot,i)||_2^2)^{\zeta}} \tag{2-10}$$

where $0 < \zeta < 1$ is a parameter that determines how strong the depth compensation is. When $\zeta = 0$, there is no depth bias compensation, on the other hand, $\zeta = 1$ leads to full compensation. For the present work, this parameters was empirically fixed as $\zeta = 0.6$.

2.3.3. Reconstruction performance measures

All the algorithms considered in this work are compared in terms of reconstruction accuracy. Specifically, to assess spatial quality of achieved activity reconstruction, the following positive semidefinite measures are used:

– *Earth-Movers Distance*, $m_e \subset \mathbb{R}^+$, that measures dissimilarity between two activity distribution, in other words, the cost of transforming the reconstructed activity into the true activity. It is defined as follows:

$$m_e = d_e\left\{\boldsymbol{J}_e, \widehat{\boldsymbol{J}}_e\right\}$$

where $\boldsymbol{J}_e \subset \mathbb{R}^{3N_d \times 1}$ is the energy of simulated activity averaged across time and $\widehat{\boldsymbol{J}_e}$ is its corresponding estimation. The lower the value of m_e, the better the achieved reconstruction.

– *Spatial Accuracy Index*, $m_a \subset \mathbb{R}^+$, that shows algorithm precision of location prediction of the true activity local maxima of reconstructed brain activity. Therefore, the higher the value of m_a, the better the achieved reconstruction. This measure is computed as $m_a = N_{t_p}/(N_{t_p} + N_{f_p})$ and requires each reconstruction dipole representing a local maximum to be labeled as either True Positive t_p or False Positive f_p. To this end, we label each local maxima of the reconstruction as t_p if the geodesic distance to a given simulated local maxima is less than some search-size. Specifically, we fix that size as 5 *cm*. Otherwise, a given local maxima of the reconstruction is labeled as f_p.

On the other hand, temporal reconstruction quality is assessed using *Maximum correlation,* $m_c \subset \mathbb{R}^+$, that is dipole-wise computed between the time series of the reconstructed activity and the simulated active dipoles. The mean over all estimated maximum correlation values is reported. In this case, the higher the value of m_c, the better the achieved reconstruction.

2.3.4. Implementation details of IRA

As dynamic constraints in the inverse problem solution, based on the DNF model presented in [6,17] (Eq. (2-3)), we consider the following two approaches:

– Linear model that does not consider the delayed state as consequence of the introduced extra-cortical loop nor non-linear terms, i.e., $a_2 = a_3 = 0$:

$$\boldsymbol{f}_l\left(\boldsymbol{j}_{k-1}, \boldsymbol{j}_{k-2}\boldsymbol{w}\right) = \boldsymbol{A}_1\boldsymbol{j}_{k-1} + \boldsymbol{A}_4\boldsymbol{j}_{k-2}, \tag{2-11}$$

with $N_p = 3$ and $\boldsymbol{w}^\mathsf{T} = \begin{bmatrix}\boldsymbol{a_1} & \boldsymbol{b_1} & \boldsymbol{a_4}\end{bmatrix}$. Hereafter, this approach is termed IRA3.

– Non-linear model that includes the non linear terms of Eq. (2-3), but it ignores the extra-cortical neural feedback (higher order lag):

$$\boldsymbol{f}_l\left(\boldsymbol{j}_{k-1}, \boldsymbol{j}_{k-2}, \boldsymbol{w}\right) = \boldsymbol{A}_1\boldsymbol{j}_{k-1} + \boldsymbol{A}_2\boldsymbol{j}_{k-1}^2 + \boldsymbol{A}_3\boldsymbol{j}_{k-1}^3 + \boldsymbol{A}_4\boldsymbol{j}_{k-2}, \tag{2-12}$$

In this case $\boldsymbol{w}^\mathsf{T} = \begin{bmatrix}\boldsymbol{a_1} & \boldsymbol{b_1} & \boldsymbol{a_2} & \boldsymbol{a_3} & \boldsymbol{a_4}\end{bmatrix}$, i.e., $N_p = 5$. Hereafter, this approach is termed IRA5.

Another aspect to be considered is the appropriate choice of the hyper-parameter values, λ and γ. Specifically, estimation of covariance matrices $\boldsymbol{Q}$ and $\boldsymbol{Q}_\epsilon$ strongly depends on the fixed regularization parameters. To this end, several methods can be used, including L-curve, General

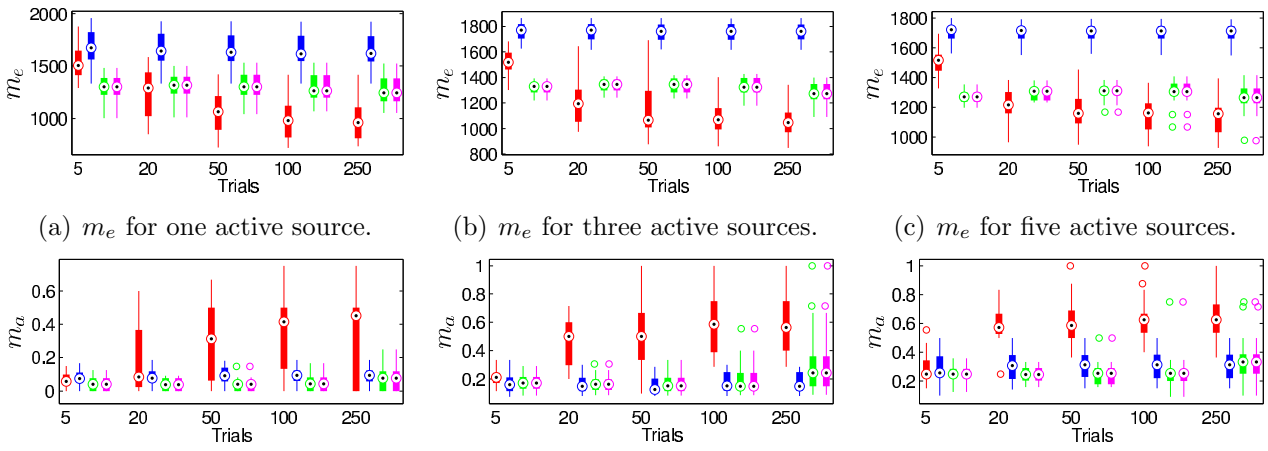

(a) m_e for one active source. (b) m_e for three active sources. (c) m_e for five active sources.

(d) m_a for one active source. (e) m_a for three active sources. (f) m_a for five active sources.

Figure **2-3**.: Spatial quality of the reconstructions obtained with: LOR_p KAL IRA3 IRA5.

Cross-Validation (GCV), and the Akaike's Bayesian Information Criterion, as described in [10,12]. Here, we calculate hyper-parameter values using the following minimization function [12]:

$$\arg\min_{\lambda,\gamma} \frac{||\boldsymbol{L}\boldsymbol{j}_k(\lambda,\gamma) - \boldsymbol{y}_k||^2}{\text{trace}(\boldsymbol{I}_{N_c} - \boldsymbol{L}\boldsymbol{T}(\lambda))^2}$$

where $\boldsymbol{T}(\lambda)$ is the inverse operator defined as $\boldsymbol{T}(\lambda) = \boldsymbol{Q}\boldsymbol{L}^\top \left(\boldsymbol{L}\boldsymbol{Q}\boldsymbol{L}^\top + \boldsymbol{Q}_\epsilon\right)^{-1}$.

2.4. Results of simulated EEG data

To assess the performance of IRA, it is compared against a Kalman filter estimation as studied in [10] and the LOR_p estimator. The latter correspond to a LORETA estimation but using only the principal components of the EEG data covariance -as explained in chapter 1.5.2-. This is to analyze the differences between explicit and implicit inclusion of temporal constraint in the EEG inverse problem.

Figure **2-3** shows the estimated spatial quality measures. According to m_e (top row), the performance of the four methods is relatively constant for different number of active sources, being the Kalman filter the method with the worst performance. For LOR_p, m_e is inversely proportional to the number of trials, i.e., SNR. This is because for low SNR, the main components identified actually correspond to noise, and not to simulated neural activity. On the other hand, Kalman and IRA estimations are much more robust to noise, however, for high SNR, LOR_p has a better performance than the other considered methods.

Regarding m_a, despite its greater dispersion, LOR_p performance is considerably better than the other methods. This means that the localization error achieved with Kalman and IRA is very high. Additionally, once again it can be seen that noise is a critical parameter for LOR_p since for low SNR it continues showing bad performance.

Regarding the temporal reconstruction quality m_c, shown in Figure **2-4**, IRA3 and IRA5 perform better than the other methods for several active sources (three and five), performing with a very

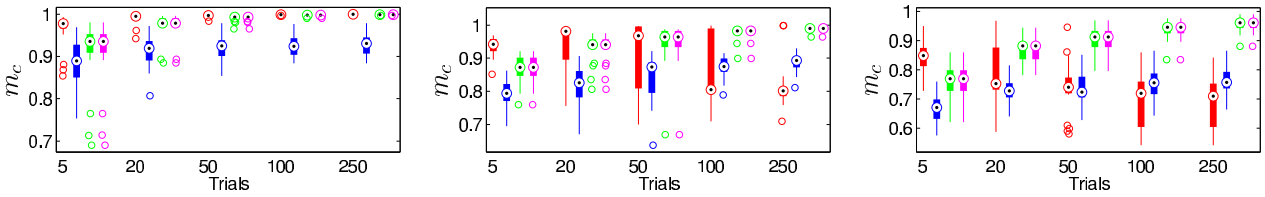

(a) m_c for one active source. (b) m_c for three active sources. (c) m_c for five active sources.

Figure **2-4**.: Maximum correlation achieved with each estimator.
■LOR$_p$ ■KAL ■IRA3 ■IRA5.

low dispersion of the results. For a single active source, the performance of IRA3 and IRA5 is equivalent to the performance of LOR$_p$. Finally, in each considered scenario, the performance of Kalman was significantly lower compared to the other considered methods.

2.5. Real EEG data

2.5.1. Database

To validate IRA Performance, two real EEG datasets are used:

- The first set is a segment extracted from a long EEG recording from a male subject (PERNC) in awake resting state, aged 24 years and diagnosed with focal epilepsy in the right frontal lobe. The EEG recording was collected during routine clinical practice at *Instituto de Epilepsia y Parkinson del Eje Cafetero*, Pereira, Colombia. The EEG signals were recorded using 34 Electrodes placed according to the 10-20 system and sampled at $1\,kHz$. The digitalized signal was subsampled at $200\,Hz$. The segment analyzed has a length of $1\,s$ and contains the beginning of an ictal event marked by the epileptologist at $t = 0\,s$. The recording begins at $t = -0.5\,s$

- The second dataset used was presented at [35] and is freely available online[1]. The original data set contains EEG recordings of 23 cases of severe epilepsy diagnosed and operated for intractable epilepsy. Since the real datasets are used in the present work to validate IRA, we utilized EEG registers of only three of the subjects to keep the scope of the work narrow enough, namely, the code names of the studied subjects are: GILPAU, NOWJON, and FRAANN. The segment analyzed has a total length of 6 seconds: 2 seconds before the ictal event ($t = 0\,s$) and 4 seconds after it.

The segments were preprocessed using a band pass filter between $0.5\,Hz$ and $25\,Hz$. Moreover, given how similar the results attained by IRA3 (linear state transition model) and IRA5 (non-linear state transition model) are in the simulated dataset, we also study if such similarity holds also for real data.
In this regard, we compared the solutions obtained for the real datasets -both Pereira dataset and EEG.PL- and obtained that the solutions are virtually the same (about $97 - 98\,\%$ of correlation

[1]The second dataset can be downloaded at `http://eeg.pl/epi`.

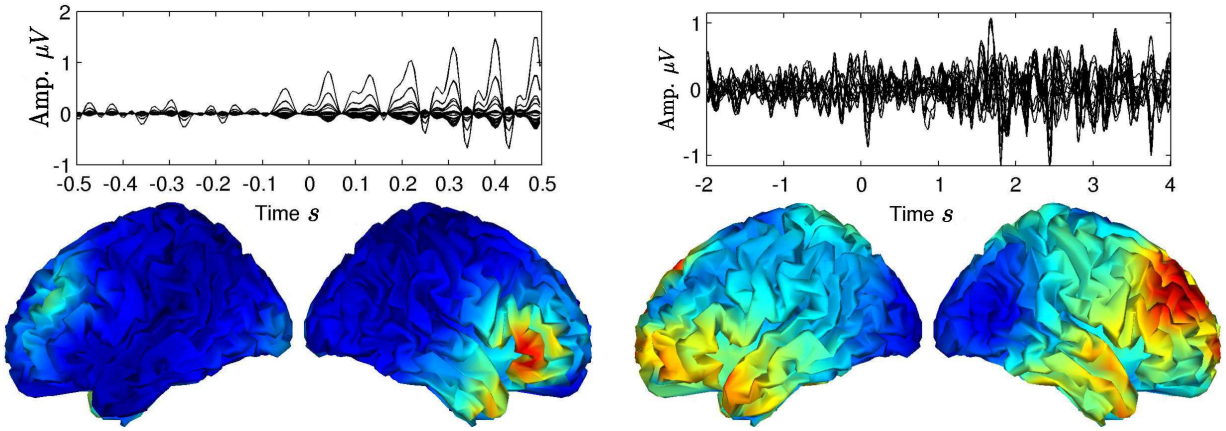

(a) Pereira dataset. Subject: PERNC. Diagnosis: Epiloptogenic focus on the right frontal lobe.

(b) eeg.pl dataset. Subject: GILPAU. Diagnosis: Cortical dysplasia in left frontal lobe.

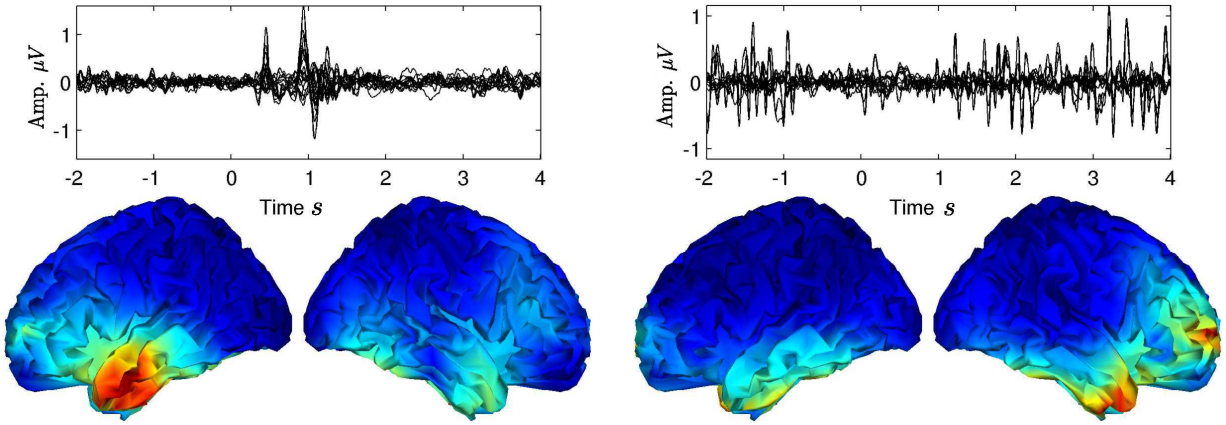

(c) eeg.pl dataset. Subject: NOWJON. Diagnosis: Mesial temporal lobe epilepsy.

(d) eeg.pl dataset. Subject: FRAANN. Diagnosis: Ganglioglioma within right hippocampus.

Figure **2-5**.: Brain mapping achieved for real data, and corresponding EEG dataset.

both in time and space domains) which confirms the hypothesis about the resemblance of the results obtained for the simulated datasets. Consequently, only IRA5 results are reported from this point onwards, because the non-linear terms may provide more information about the underlying processes.

2.5.2. Results

Figure **2-5** shows the real EEG segments considered in the present study and the averaged activity obtained with IRA5[2].

Regarding the results obtained for PERNC, IRA5 succesfully localize the epileptogenic focus in the right temporal lobe, although some spurious activity appeared in the right temporal lobe and in the left temporal lobe, probably related with the head model and residual noise in the EEG signals.

[2]Average is taken from $t = -2\,s$ to $t = 0\,s$

Furthermore, mapping achieved for NOWJON localized the pathological tissue in the left temporal lobe, which is the area removed during the surgical treatment. Traces of activity are also present in the right temporal lobe.
Mapping obtained for subject FRAANN shows activity mainly in the right temporal and frontal lobes. Such reconstruction agrees with the description made by the epileptologist: "EEG - interictal - showed some repetitive synchronous spiking within right fronto-temporal region".
Finally, for GILPAU the reconstruction was not as accurate as in the other methods. In this case, activity appears all over the brain, except in the occipital lobes, the highest spatial peak of activity is located in the right temporal lobe even when the focus was diagnosed in the left frontal lobe.
Moreover **2-6** shows the DNF parameters corresponding to the brain mappings obtained for real data. One of the main objectives of the proposed method was to identify different states (in this case pathological/non-pathological) by analyzing the model parameters. In some cases, specifically for GILPAU and PERNC, the linear parameters (a_1, b_1 and a_4) show a change in the convergence rate just in the time instant marked as the begin of the ictal event ($t = 0$). However, for NOWJON and FRAANN, this is not evident enough and strong conclusions cannot be made. Furthermore, it would be expected that non linear parameters a_2 and a_3 would provide a deeper understanding of the underlying process. However, such parameters are the ones that contribute the less to the model (virtually zero for the whole EEG segment). Also, even if such parameters are zoomed in, there are no specific and/or conclusive behavior(central and right columns of Figure **2-6**).

2.6. Discussion

The proposed IRA method deals with the inclusion of information about the neural activity generation model but also taking into account the dynamics of the model themselves. One of the aspects that requires important consideration is the selection of the model that describes the neural activity. Naive approaches have been taken in the past, for example by selecting random walk models [27], or second order linear models [3, 10]. However, such models may not suffice to fully describe complex dynamics found in EEG recordings.
To study the impact of the brain activity dynamic model in the EEG inverse problem solution, two versions a DNF-based model are used to provide the solver with dynamic constraints compatible with the problem at hand. The two versions correspond to a linear and a non-linear approximation of the original DNF-model. This allows to test the hypothesis of whether the inclusion of non linear terms improves the final reconstruction and considerably contributes to the identification of the neural-activity generation model.
Results show that the differences between the linear and non-linear model is not significant. However, the inclusion of a time-varying model to describe changes in the brain dynamics improves reconstruction accuracy in both temporal and spatial domains, at least compared with the time-invariant model considered in the Kalman Filter solution used in [3, 10].
Furthermore, given that it is unlikely that all mental states and brain dynamics can be simple enough to be described by a single non-linear model (as George Box once said "all models are wrong, but some are useful"), we compared the proposed approach with a standard method - LORETA- using only N_q main temporal components of the data to constrain the estimation in the

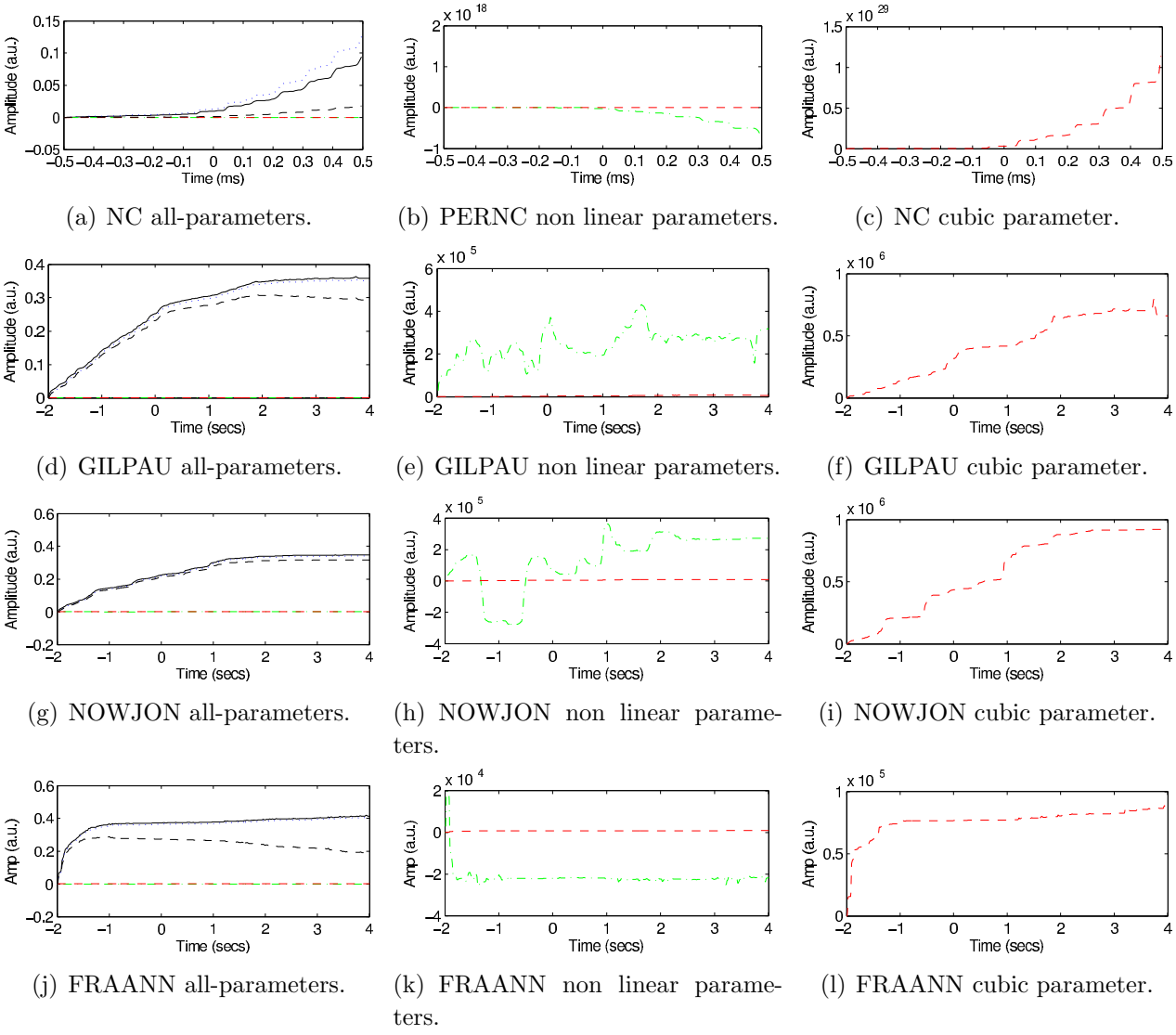

(a) NC all-parameters. (b) PERNC non linear parameters. (c) NC cubic parameter.

(d) GILPAU all-parameters. (e) GILPAU non linear parameters. (f) GILPAU cubic parameter.

(g) NOWJON all-parameters. (h) NOWJON non linear parameters. (i) NOWJON cubic parameter.

(j) FRAANN all-parameters. (k) FRAANN non linear parameters. (l) FRAANN cubic parameter.

Figure **2-6**.: Parameters computed for each of the studied subjects. Left most columns shows all the parameters, while the column in the middle and the right most column show, respectively, only non linear and cubic parameters for the sake of clarity.
$-a_1$ $\cdots b_1$ $-\cdot-a_2$ $-\,-a_3$ $-\;-a_4$.

time-domain, (see LOR_p in Chapter 1.5.2). In this regard, the results show that using automatically identified temporal components -LOR_p- yields better performance measures than explicitly constraining the solution through a state space model, using either static (Kalman) or time-variant linear/non-linear (IRA3 and IRA5) approximations of the DNF-based model. Nevertheless, such results only hold for signals with high SNR.
An other aspect that is important to analyze is the temporal evolution of the DNF-based model parameters. One of the main purposes of IRA -besides improving the reconstruction quality- is to dynamically model the neural activity generators and identify its different states. This topic should be directly assessed in real data since simulated data does not offer sufficient interpretability to provide a conclusion. The temporal evolution of the model parameters during the analysis of the real EEG segments allows to infer that IRA identifies changes of the activity generators, at least to distinguish pathological from non-pathological states related with epilepsy. Both linear and non-linear model do not show any differences in the results attained in this regard. Which means that the non-linear terms do not truly help to model brain dynamics and raises another reason to believe that constraining the temporal components of the reconstruction through implicit structures -as done in LOR_p- is more appropriate than fixing a deterministic structure -as in Kalman, IRA3 and IRA5-.

2.7. Summary

An Iterative Regularization Algorithm -IRA- has been proposed to improve the accuracy of brain activity reconstruction through a time-varying state space model to explicitly constrain the dynamics of neural activity. IRA has been compared to another state-space based framework proposed in [10] and further studied in [3]. Results show that there is an improvement with respect to this state space-based method. However, compared to implicit data driven temporal constrained methods (LOR_p), IRA does not perform better. The second objective of IRA was to use the estimated model hyperparameters to identify and describe changes in the dynamics of neural activity generators. IRA succeeded in the identification and modeling of pathological and non-pathological epilepsy-related events in some patients, although a strong conclusion cannot be claimed in this regard. In general IRA has regular reconstruction accuracy and the estimate DNF-model parameters does not provide a strong insight about the brain activity generation model. However, the latter topic should be further explored with different real data.

3. Dynamic spatial constraints for non-stationary brain activity reconstruction - DOBERMAN

3.1. Introduction

One of the physiologically fostered assumptions typically made in the solution of the EEG inverse problem is that brain activity can be represented through a small/sparse set of spatial basis functions (termed spatial blobs or patches), that is, the constrained solution is a linear combination of some predefined spatial patches. The following patch-based approaches are the most representative in the state of the art: Automatic Relevance Determination (ARD) , Greedy Search (GS) [8], Multiple Sparse Priors (MSP) [9], Sparse Basis Field Expansion (S-FLEX) [14]. Yet, such methods assume that the active brain areas remain the same throughout the entire solution interval [11]. This assumption is far from being totally realistic in many practical scenarios, where brain activity has strong spatio-temporal dynamics and may be non-stationary [11, 17].
The proposal presented in this chapter assumes that brain activity can be represented by a set of small and locally smooth spatial patches, but relaxing the assumption about the stationarity of the problem by using time-varying prior knowledge -introduced as a time varying a-priori covariance matrix-. Specifically, our method is comprised of the following two stages: *i*) computation of a locally smooth spatial dictionary where each element represents brain areas potentially generating a set of pre-identified dynamics, *ii*) Linear combination of the spatial dictionary elements, which is modeled as a time-varying process. Obtained results on simulated and real EEG databases show that the proposed method improves the quality of brain activity reconstruction and provides important interpretability of the solution through the estimated time varying components of the solution.

3.2. Materials and Methods

3.2.1. Time varying priors in a Bayesian estimation framework

Though ARD, GS, MSP and S-FLEX provide a well-structured spatially sparse solution -which is a physiologically meaningful feature-, their estimator completely ignores temporal EEG data information and rather they assume that activity of certain brain areas remain active during the whole analysis interval. To improve estimation quality of the solution, we develop the Dynamically cOnstrained BRain MAppiNg approach, termed DOBERMAN, that makes the following assump-

tions about the stochastic model of neural activity: *i*) It occurs over a small number of localized brain regions, as assumed in ARD, GS, MSP and S-FLEX, and *ii*) it presents non-stationary temporal dynamics that can be measurable in the second statistical moment (variance). Therefore, we obtain an adaptive prior, $\boldsymbol{Q}$, that encodes temporal changes of neural activity, while keeping spatial coherence by also using a spatial dictionary $\boldsymbol{\Phi}_s$. The developed approach splits the solution into the following two stages:

3.2.2. Time and spatial dynamics computation

First, N_q main temporal components are extracted from original input data by using the first N_q eigenvectors of the temporal covariance matrix that is obtained from its SVD decomposition $\boldsymbol{V}\boldsymbol{S}\boldsymbol{V}^{\mathsf{T}}=\boldsymbol{Y}^{\mathsf{T}}\boldsymbol{Y}$, where $\boldsymbol{V} \subset \mathbb{R}^{N_t \times N_t}$ is a matrix for which each column corresponds to the right singular vectors (temporal components) of $\boldsymbol{Y}$, and $\boldsymbol{S} \subset \mathbb{R}^{N_t \times N_t}$ is a matrix holding in the main diagonal its corresponding eigenvalues.

Afterwards, a reduced spatial dictionary, $\boldsymbol{\Phi}_s^*$, is selected from the original set $\boldsymbol{\Phi}_s$ by estimating activity generated by the temporal decomposition explained above. Each element of the reduced spatial set is calculated using the S-FLEX method, that is, $\{\boldsymbol{\Phi}_s^*(\cdot, i) = \mathrm{S-FLEX}\left(\boldsymbol{\Phi}_s, \boldsymbol{Y}\boldsymbol{V}_{(\cdot,i)}\right) : \forall i \in N_q\}$, where $\boldsymbol{V}_{(\cdot,i)}$ holds the i-th main temporal EEG data component. However, each ith element must hold just one well defined spatially coherent generator. So, to avoid elements in $\boldsymbol{\Phi}_s^*$ holding several cortical patches, a k-means clustering algorithm is applied to properly determine each generator as independent elements of the new dictionary. As a result, we obtained a reduced spatial dictionary of size $N_r \geq N_q$.

3.2.3. Computation of time varying hyperparameters

Given the i-th element of $\boldsymbol{\Phi}_s^*$, its corresponding hyperparameter at time instant k, h_i^k, is recursively calculated using the EEG covariance computed at a fixed time window centered at time instant k. Namely, to estimate the temporal hyperparameter dynamics, a random walk model is considered, within the following state space framework:

$$h_i^k = h_i^{k-1} + \mu_i^k, \ \forall i \in N_r \tag{3-1a}$$

$$\mathrm{vec}\left(\mathrm{cov}\left(\boldsymbol{Y}^k\right)\right) = \mathrm{vec}\left(\boldsymbol{L}\boldsymbol{Q}^k\boldsymbol{L}^{\mathsf{T}}\right) + \boldsymbol{\gamma}^k \tag{3-1b}$$

where $\mathrm{vec}\,(\cdot)$ is the argument vectorization, $\mathrm{cov}\left(\boldsymbol{Y}^k\right)$ is the covariance of the window $\boldsymbol{Y}$, centered at time instant k, both μ^k and $\boldsymbol{\gamma}^k \subset \mathbb{R}^{N_c^2 \times 1}$ are measures of noise that are assumed to be normally distributed with scaled identity covariance matrices, and the time varying prior covariance matrix $\boldsymbol{Q}^k$ is defined as $\boldsymbol{Q}^k = \sum_{i \in N_r} h_i^k \boldsymbol{\Phi}_s^*(\cdot, i)$.

To estimate the hidden states in Eq. (3-1a) and (3-1b), the model can be rewritten by applying the relationship between the Kronecker product (represented as $\otimes$) and the $\mathrm{vec}\,(\cdot)$ operator as follows:

$$\boldsymbol{h}^k = \boldsymbol{h}^{k-1} + \boldsymbol{\mu}^k \tag{3-2a}$$

$$\mathrm{vec}\left(\mathrm{cov}\left(\boldsymbol{Y}^k\right)\right) = \boldsymbol{L} \otimes \boldsymbol{L}\mathrm{vec}\left(\boldsymbol{Q}^k\right) + \boldsymbol{\gamma}^k \tag{3-2b}$$

Under this formulation, the hidden states $\boldsymbol{h}^k$ are estimated using a standard Kalman filter. Then, we carry out the final mapping using the temporal signatures determined at the beginning of the whole process using $\widehat{\boldsymbol{J}}_p = \boldsymbol{Q}_p \boldsymbol{L}^\top (\boldsymbol{Q}_\epsilon + \boldsymbol{L}\boldsymbol{Q}_p\boldsymbol{L}^\top)^{-1}\boldsymbol{Y}_p$
where $\boldsymbol{Y}_p = \boldsymbol{Y}\boldsymbol{V}$ and $\boldsymbol{Q}_p = \sum_{i\in N_r} \boldsymbol{h}_i \boldsymbol{V}\boldsymbol{D}_i \subset \mathbb{R}^{3N_d \times 3N_d}$, where $\boldsymbol{h}_i$ is the time series of the i-th hyperparameter. This means that the reconstruction is obtained by projecting the original data and the time-varying hyperparameters into the main temporal components $\boldsymbol{V}$. Lastly, the final reconstruction is projected back onto the original space, that is, $\widehat{\boldsymbol{J}} = \widehat{\boldsymbol{J}}_p \boldsymbol{V}^\mathsf{T}$.
Figure **3-1** shows the schematic representation of DOBERMAN, including brain activity simulation with different number of active dipoles, temporal decomposition, clustering stage and estimation of time varying hyperparameters.

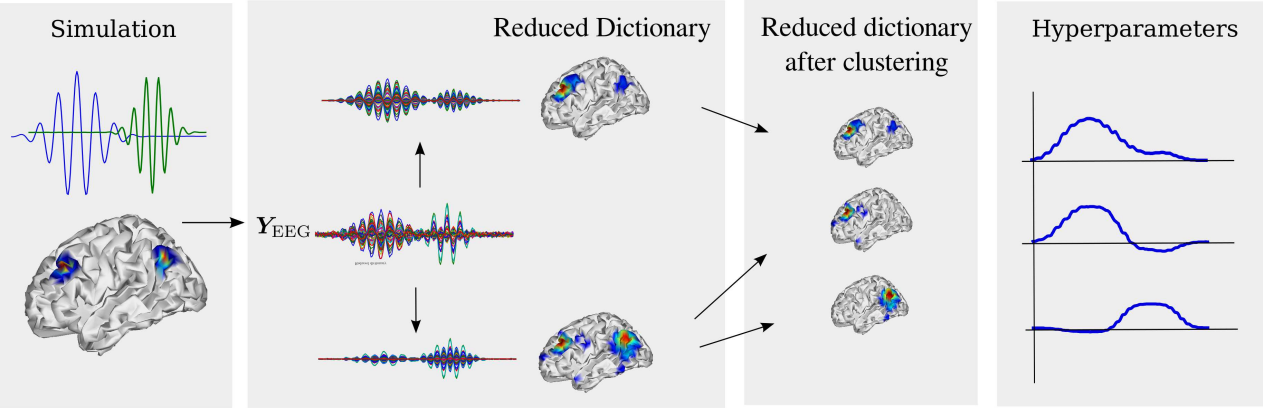

Figure **3-1**.: Illustrative example of DOBERMAN.

3.3. Experimental Setup

DOBERMAN is compared with a baseline method (LOR_p), and with two additional methods that have in common the use of a predefined set of spatial basis functions to describe brain activity, namely, S-FLEX and GS.

3.3.1. Implementation details of DOBERMAN

The parameters used in *DOBERMAN* are selected as follows:

- *Temporal decomposition*: The N_q temporal components to be used are selected to get, at least, 90% of the estimated raw data variance.

- *Clustering stage*: The standard k-means algorithm is applied on the dipoles with non-zero activity. Each (i, j) element of the affinity matrix $\boldsymbol{K}$ used in the k-means algorithm is computed using an exponential kernel, $w_{i,j} = \exp\left(-d_g\{\boldsymbol{x}_i, \boldsymbol{x}_j\}^2/\sigma^2\right)$, where σ is fixed to $5\,cm$ and $d_g\{\boldsymbol{x}_i, \boldsymbol{x}_j\}$ stands for the spatial geodesic distance between the dipoles located respectively at coordinates $\boldsymbol{x}_i$ and $\boldsymbol{x}_j$. Moreover, the number of clusters to be found is the number of eigenvalues of the affinity matrix that explain at least the 90% of the variance.

– *State space model of the hyperparameter vector* $\boldsymbol{h}$: The window used to compute the covariance of matrix $\boldsymbol{Y}_k$ is centered at time instant k and its length is set as N_c to get a full rank matrix. Additionally, Both covariances of noise processes, $\boldsymbol{\mu}$ and $\boldsymbol{\gamma}$, are set as identity matrices.

– *Spatial dictionary*, $\boldsymbol{\Phi}_s$, is built in the form of Gaussian functions that are placed at every discrete dipole:

$$\boldsymbol{\Phi}_s(i,j) = \exp\{-d_g\{\boldsymbol{x}_{(i)}, \boldsymbol{x}_{(j)}\}^2/\sigma^2\},$$

where $\boldsymbol{\Phi}_s(i,j) \subset \mathbb{R}^+$ is the value of the i-th element of the dictionary at jth dipole, $d_g\{\boldsymbol{x}_{(i)}, \boldsymbol{x}_{(j)}\} \subset \mathbb{R}^+$ is the geodesic distance along the cortical surface between i-th and j-th dipole, $\sigma \subset \mathbb{R}^+$ is the width of every used Gaussian function. The σ is to be selected to get solutions having adequate spatial resolution (i.e., narrow functions), but at the same time, as to promote local smoothness (i.e., wide functions). In the concrete case, this value is heuristically fixed as $\sigma = 1\,cm$. It is worth noting that such spatial dictionary was also used in S-FLEX and GS.

3.4. Results of simulated EEG data

Figure **3-2** shows estimated measures of spatial quality estimated for the considered mapping methods. Regarding m_e -top row-, for a single active source, S-FLEX outperforms the other methods resulting also in low dispersion of the results. However, for several active sources, the performance of S-FLEX remains constant but DOBERMAN significantly improves, maintaining its low dispersion. Regarding GS, it has a good performance, although it is significantly worse than S-FLEX and DOBERMAN. Lastly, LOR_p is the method with the worse performance and bigger dispersion, and also, it is the method that is more sensitive to noise.

In terms of the spatial accuracy index m_a, DOBERMAN has the best performance among all considered methods when several sources are active, specially for high SNR. Nevertheless, for a single active source, S-FLEX and GS achieved the best performance, although the dispersion of the results is considerably higher than the other methods. For a single source, DOBERMAN has a considerably low performance, even worse that LOR_p in some cases. Also, under this measure, LOR_p has a similar performance compared to the other methods under high SNR, however, for low SNR, its performance is heavily hindered.

According to the temporal reconstruction quality shown in Figure **3-3**, DOBERMAN has the worst performance under every considered condition, mainly when several sources are active in the simulation. Under this measure, there does not exist a method with outstanding performance. However, the methods based on spatial dictionaries have the steadiest performance -reflected with the low dispersion in the m_c values obtained-, while LOR_p -the only method not using spatial dictionary- has a significantly higher dispersion.

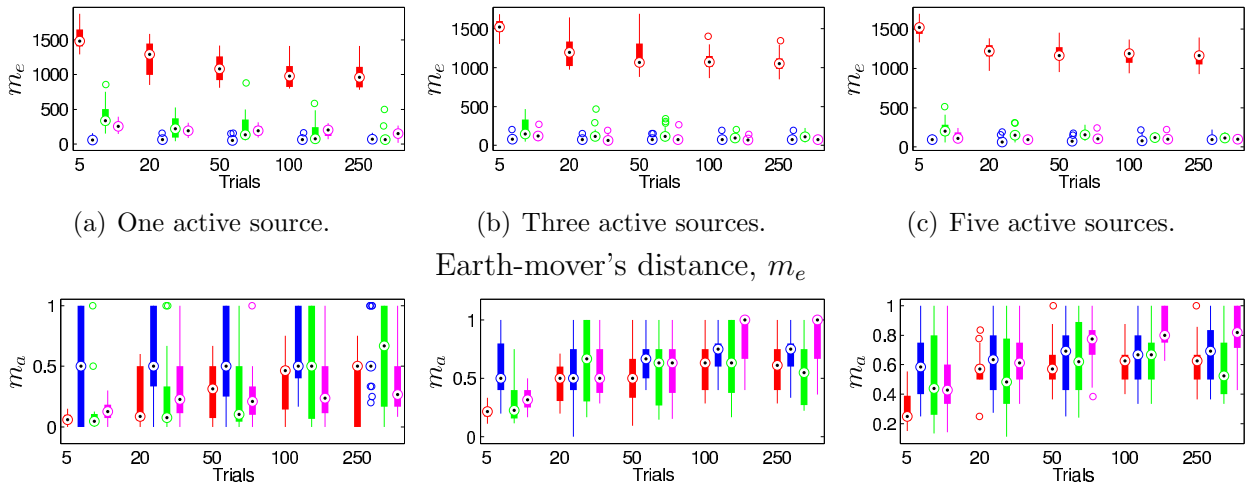

(a) One active source. (b) Three active sources. (c) Five active sources.

Earth-mover's distance, m_e

(d) One active source. (e) Three active sources. (f) Five active sources.

Spatial accuracy index, m_a

Figure **3-2**.: Spatial quality of reconstruction achieved by:
■LOR$_p$ ■S-FLEX ■GS ■DOBERMAN.

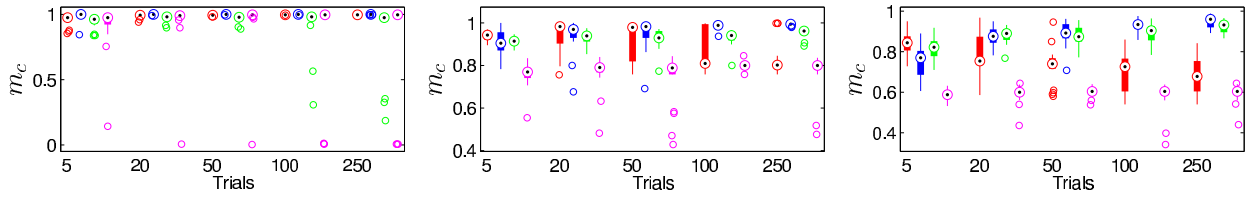

(a) one active source. (b) three active sources. (c) five active sources.

Figure **3-3**.: Temporal quality of reconstruction for:
■LOR$_p$ ■S-FLEX ■GS ■DOBERMAN.

3.5. Real EEG data

3.5.1. Database

Real EEG data used to validate the DOBERMAN algorithm is a standard auditory odd-ball experiment presented in [16]. Although, the data collection holds 12 subjects, we just consider 10, which are all healthy, with normal hearing, non-smokers, aging in the range of 21 to 34. All subjects were asked to count a target stimuli while ignoring a non-target one in the context of an online spelling task. The stimuli, which last $100\,ms$, are separated from each other in $225\,ms$. In average, 450 trials for non-target stimuli and 120 trials for target stimuli were available per subject. EEG signals were recorded monopolarly using 63 wet electrodes placed at symmetrical positions according to the international $10-20$ system. Channels were referenced to the nose. The hardware sampling rate was $1\,kHz$ and the signal was further sub-sampled at $200\,Hz$. As preprocessing stage, the data was band-pass filtered between 0.4 and $25\,Hz$.

3.5.2. Results

Figures **3-4** and **3-5** show some examples of reconstructed responses to target and non-target stimuli, respectively, estimated for one subject. Both Figures also display the estimated scalp maps based on the measured EEG data, the time series of the averaged trials as well as the reduced spatial dictionaries used to perform the reconstruction, and the corresponding hyperparameters. Although it may be hard to draw a strong conclusion from the estimated scalp map, yet achieved reconstruction shows activity located on the area right above the lateral sulcus at $150\,ms$ after the beginning of the stimulus time, as seen in Figure **3-4**. This activity is linked to the N180 ERP. On the other hand, for the target stimuli response shown in Figure **3-5**, auditory cortex remains active as well as other sources now appearing in the frontal lobe that is one of the brain areas associated with conscious processing of stimuli.

Furthermore, regarding the analysis of the spatial dictionary used to perform the reconstruction, Figure **3-4** shows that for non target stimuli the two auditory cortices are spatially distinguished an represented separately into a couple of different dictionary elements. Also, the hyperparameter time series related to auditory cortex dictionary elements holds some periodical peaks every $225\,ms$ that is actually the interval between stimuli. Thus, we may infer that the DOBERMAN algorithm allows identifying the dynamics associated with the stimulus response (in this case, the N180 ERP). In case of the target stimuli, obtained reconstruction shows that the most significant dictionary elements are not only related to the auditory cortex, but also to the frontal lobe. In this instance, the estimated time series $\boldsymbol{h}$ brings just a single peak at approximately $150\,ms$ and then another at $300\,ms$; both maximum points may be correlated the N150 and P300 ERP, respectively.

Figure **3-6** (top row) shows the averaged brain activity computed for all subjects that took part of the experiment. The localization of the auditory cortex is noisy because of the anatomical differences among subjects, as well as the localization of the electrodes of the scalp may have differ between each experiment. The average achieved for non-target stimuli shows strong activity in the area surrounding the auditory cortex, namely, the lateral sulcus and the superior temporal gyri. On the other hand, for target stimuli, the energy of the activity in the auditory cortex remains

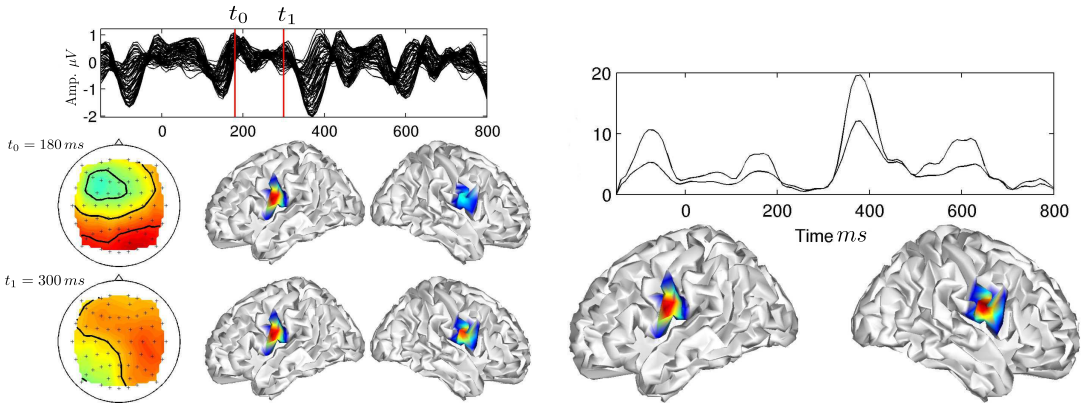

(a) Brain activity reconstruction. Top: Time series of the averaged trials. Left: Scalp maps computed for the averaged trials. Middle and right: Different views of the reconstruction achieved at two different time instant indicated with two vertical lines in the top plot.

(b) Most significant elements of the spatial dictionary and hyperparemters for the complete dictionary.

Figure **3-4**.: Brain activity reconstruction attained for non-target stimuli response of subject 6 and the corresponding spatial dictionary used in the reconstruction.

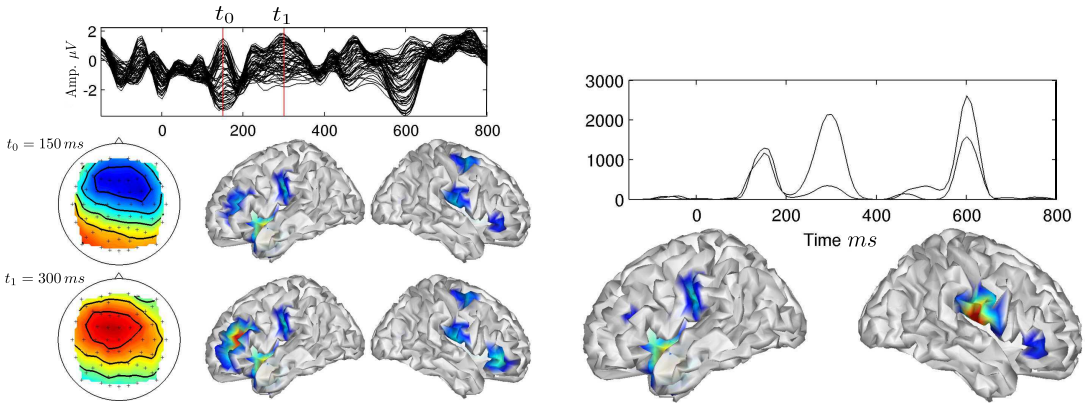

(a) Brain activity reconstruction. Top: Time series of the averaged trials. Left: Scalp maps computed for the averaged trials. Middle and right: Different views of the reconstruction achieved at two different time instant indicated with two vertical lines in the top plot.

(b) Most significant elements of the spatial dictionary and hyperparemters for the complete dictionary.

Figure **3-5**.: Brain activity reconstruction attained for target stimuli response of subject 6 and the corresponding spatial dictionary used in the reconstruction.

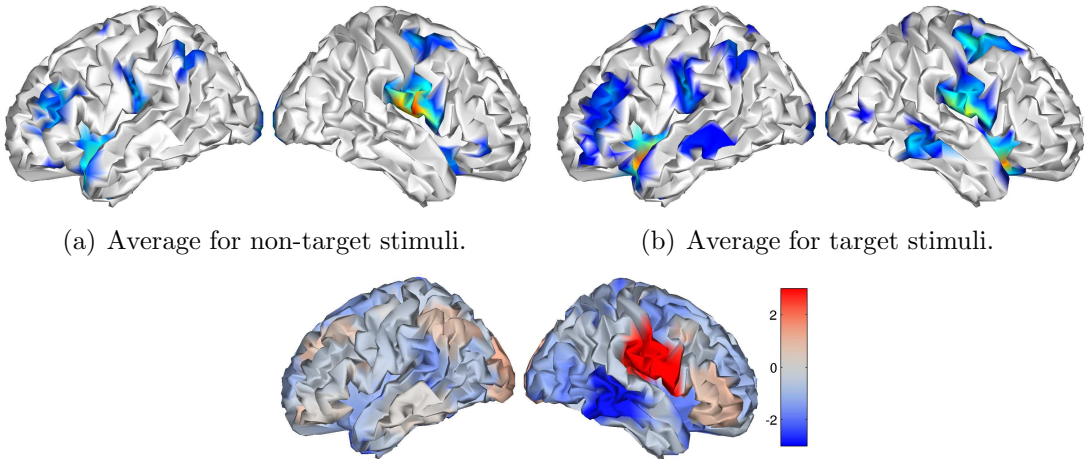

(a) Average for non-target stimuli.

(b) Average for target stimuli.

(c) T-test scores.

Figure **3-6**.: Average of mapping across subjects for target and non-target stimuli, with the corresponding T-test score for each dipole to compare differences between active brain areas during target and non-target stimuli

but decreases, and several sources appear spread over the cortex, mainly the frontal and parietal lobe.

Lastly, to make clear the differences among brain areas activated by either target or non-target stimuli, we carry out the t-student test on each discrete dipole. So, as displayed in **3-6** (bottom), provided statistical test reaffirms those findings achieved above by visual inspection, i.e., one of the statistical groups stands for activity surrounding the auditory cortex (colored in red), although this is only evident in the right hemisphere.

3.6. Discussion

The proposed method -DOBERMAN- addresses the reconstruction of non-stationary brain activity by introducing a set of spatio-temporal constraints within the standard Bayesian framework. To this end, we initially carry out a plain temporal decomposition of input EEG data to produce the dictionary encoding existing spatial dynamics. Then, we introduce a set of time varying hyper-parameters dynamically weighting spatial patches that provides the spatio-temporal constraints to be used in the inverse problem solution.

One of the critical stages in the proposed method is the identification of the main temporal dynamics of the data. In the proposed approach we carry out this task with an SVD decomposition. It has been shown that for high SNR, this approach is appropriate, however, if the SNR decreases, the performance of DOBERMAN is expected to worsen due to the high sensibility of the SVD with respect to the energy of the noise, i.e., for low SNR, the components identified as relevant may correspond to noise. The SVD decomposition was used to due its relative simplicity and affordable computational burden. In the analyzed scenarios, this decomposition was enough to identify the main dynamics present both in simulated and real data. However, if we expect that the most complex dynamics of the EEG data may not be fully identified with this naive approach

-or if available data is too noisy-, the proposed method is transparent to the decomposition used to identify the critical temporal components of brain activity dynamics. In this regard, for example, a time frequency decomposition could be utilized. However, exploration of such diversity of potential techniques is out of the scope of the present work.

Regarding the spatial basis functions to constraint the spatial distribution of reconstructed activity, unlike the baseline methods S-FLEX and GS where certain active areas are encouraged to appear in the solution during the entire time window of analysis, our contribution lies on the fact that these spatial constraints are expressed dynamically in time. As a result, our algorithm includes in the solution all concrete activated brain areas depending on the dynamics captured by the estimated main temporal components. However, to ensure that each specific area corresponds to an individual, focal structure,the clustering stage must be also included since the computed temporal signature set may hold information about different clusters of activity. In the concrete case, the k-means clustering algorithm is applied to determine properly each generator as an independent element of the new dictionary. This proved to be one of the sensitive stages of DOBERMAN. Specifically, the number of clusters and the bandwidth of the Gaussian kernel should be carefully tuned, otherwise, spurious sources may begin to appear if too many clusters are assumed or if the bandwidth of the kernel is too narrow.

To assess the EEG inverse solution, validation of the proposed DOBERMAN algorithm is firstly carried out on simulated data. As a result, quality measures estimated activity allows inferring that the DOBERMAN algorithm mainly outperforms LOR_p and GS. Furthermore, with respect to S-FLEX, DOBERMAN is slightly superior in some scenarios, although, a strong conclusion cannot be drawn in this regard.

Regarding the results of DOBERMAN in the real ERP data showed that the proposed method is capable of correctly reconstructing realistic brain activity. Moreover, one of the main advantages is that the hyperparameters weighting each element of the reduced spatial dictionary are highly interpretable and may provided a greater insight about the spatial dynamics of the data. Specifically, for ERP data, the peaks corresponding to the activation of different brain areas can be easily seen, and are associated with each of the stages of the perception stream.

3.7. Summary

In this chapter, we presented a novel method -termed DOBERMAN- which allows to relax the stationarity assumption in the solution of the EEG inverse problem. This is achieved by including in the standard Bayesian solution framework a time varying a priori covariance matrix of the brain activity. Furthermore, to ensure that the solution has a physiologically meaningful distribution, the proposed time varying covariance matrix is assumed to be composed of a set of well defined spatial basis functions. Furthermore, to decrease the computational burden of the algorithm, only a small set of spatial basis functions is used, such basis functions are the result of brain mappings corresponding to the main dynamics identified through an SVD. In this regard, it has been shown that for specific values of SNR, the SVD decomposition is not robust enough. Finally, for real data it has been shown that the weighting hyperparameters computed for each element of the spatial dictionary are highly interpretable and may be easily related to different brain states, depending

on the studied neurological phenomenon.

4. Reconstruction of non stationary activity using space-time-frequency dictionaries - STOUT

4.1. Introduction

As stated throughout the present work, brain activity may be non-stationary for sufficiently long EEG measures. Besides that, it has been shown the importance of obtaining a spatially coherent solution which can be achieved by representing brain activity through a set of locally smooth spatial basis functions. Two state of the art methods separately address such physiologically meaningful constraints. Namely, Sparse Basis Field Expansion (S-FLEX) [14] regards with the representation of brain activity using a set of focally sparse spatial basis functions (spatial coherence), while Time-Frequency Mixed Norm Estimate (TF-MxNE) [11] addresses the non stationarity issue by representing brain activity through a set of time-frequency basis functions. Inspired by TF-MxNE and S-FLEX, we introduce a novel method to obtain a solution that handles spatial coherence -as S-FLEX- and sparse time-frequency representations of the solution -as TF-MXNE-.
In the approach proposed in the present chapter we assume that brain activity may be represented by a joint-linear combination of physiologically plausible spatial and temporal basis functions, fostering brain activity reconstruction with spatial coherence but also considering the non stationarity and complex dynamics that may be found in EEG recordings.

4.2. Materials and Methods

As stated before, the non-stationary nature of brain activity poses a major challenge to robust brain mapping. Furthermore, algorithms that place spatial sparsity constraints directly in the source space may lead to unstable and scattered solutions. To cope with both issues, we introduce the Spatio-TempOral Unifying Tomography (STOUT), which supplies a generalized solution handling jointly spatial-coherence and time-frequency sparsity. For this purpose, as proposed in [11], prior information about brain activity $\boldsymbol{J}$ may be written as a combination of both time and spatial dynamics in the form:

$$\Theta\left(\boldsymbol{J}\right) = \Theta_s\left(\boldsymbol{J}\right) + \Theta_t\left(\boldsymbol{J}\right) \tag{4-1}$$

where $\Theta_s\left(\boldsymbol{J}\right)$ and $\Theta_t\left(\boldsymbol{J}\right)$ are the energy functions associated with specific spatial and temporal dynamics, respectively.

Although there are several approaches that yield sparse solutions in either time or space domains, we based our method (STOUT) on SFLEX and TF-MxNE algorithms since both approaches are based on physiologically motivated priors, expanding the current density into spatial or temporal sparse basis fields, respectively. Consequently, we propose to represent brain activity $\boldsymbol{J}$ as a single linear combination of basis functions holding joint spatio-temporal EEG data dynamics. Particularly, based on introduced sparse basis fields S-FLEX and TF-MxNE, we express brain activity in terms of the following joint space-time-frequency dictionaries:

$$\boldsymbol{J} = \boldsymbol{\Phi}_s \boldsymbol{C} \boldsymbol{\Phi}_t, \tag{4-2}$$

where $\boldsymbol{C} \subset \mathbb{C}^{N_s \times N_t}$ is the matrix holding the coefficients of the proposed linear combination. Furthermore, as done in TF-NxNE, the Laplacian priors should be placed in $\boldsymbol{C}$ to encourage time-freqency sparsity and spatially coherent solutions, i.e, $\Theta\left(\boldsymbol{C}\right) = \lambda_s ||\boldsymbol{C}||_{1,2} + \lambda_t ||\boldsymbol{C}||_1$. Accordingly, based on assumptions shown in Eq. (4-1) and (4-2), the present formulation leads to the following optimization problem:

$$\arg\min_{\boldsymbol{C}} \{||\boldsymbol{Y} - \boldsymbol{L}\boldsymbol{\Phi}_s \boldsymbol{C} \boldsymbol{\Phi}_t||_F^2 + \lambda_s ||\boldsymbol{C}||_{1,2} + \lambda_t ||\boldsymbol{C}||_1\} \tag{4-3}$$

As a result of selecting a small subset of the spatial and time frequency dictionaries $\boldsymbol{\Phi}_s$ and $\boldsymbol{\Phi}_t$ -which is achieved with the ℓ_1 and $\ell_{1,2}$ norms-, the STOUT technique fosters brain activity reconstruction represented through coherent and physiologically meaningful spatio-temporal sparse basis fields.

As regards optimization of the objective function shown in Eq. (4-3), the mathematical formulation is equivalent to one given in Eq. (1-9) for the TF-MxNE method. In other words, provided the following linear transformation, $\boldsymbol{L}' = \boldsymbol{L}\boldsymbol{\Phi}_s$, of the TF-MxNE lead field matrix, convexity of problem in Eq. (4-3) supplies also the existence of optimal solutions. Thus, the optimizer used in the TF-MxNE algorithm may also be used in our approach. Namely, we use the Fast Shrinkage Thresholding Algorithm (FISTA) [4]. The resulting optimization procedure can be seen in the algorithm 1 that relies on the given $(\ell_{1,2} + \ell_1)$-norm proximity operator defined as follows [11]:

$$\text{prox}_{\ell_1+\ell_{1,2}}\left(\boldsymbol{X}\right) = \frac{\boldsymbol{X}_{(i,j)}}{|\boldsymbol{X}_{(i,j)}|} \left\{|\boldsymbol{X}_{(i,j)}| - \lambda_t\right\}_+ \left(1 - \frac{\lambda_s}{\sqrt{\sum_{\forall i \in N_f} \left\{|\boldsymbol{X}_{(i,j)}| - \lambda_t\right\}_+^2}}\right)$$

where operator $\{\cdot\}_+$ yields the maximum value between the argument and 0, $\boldsymbol{X}_{(i,j)}$ is the value corresponding to the i-th row and j-th column of the buffer matrix $\boldsymbol{X} = \lambda_s \boldsymbol{\Phi}_s \boldsymbol{L}^\intercal (\boldsymbol{Y} - \boldsymbol{L}\boldsymbol{\Phi}_s \boldsymbol{C} \boldsymbol{\Phi}_t^{\mathbb{H}}) \boldsymbol{\Phi}_t$, with $\boldsymbol{X} \subset \mathbb{R}^{N_d \times N_f}$, that is the proximity operator argument, being $|\cdot|$ is the absolute argument, and $\boldsymbol{\Phi}_t^{\mathbb{H}}$ is the Hermitian transpose of $\boldsymbol{\Phi}_t$.

4.3. Experimental setup

4.3.1. Implementation details of STOUT

To achieve optimal brain activity reconstruction, two main issues are to be considered during implementation of the STOUT mapping algorithm: parameter tuning and construction of the

Algorithm 1 Used FISTA algorithm to optimize the STOUT method

Require: $\boldsymbol{Z} = \boldsymbol{0}$, all-zero matrix $\boldsymbol{Z} \subset \mathbb{C}^{N_s \times N_f}$
Ensure: $\boldsymbol{X} = \lambda_S \boldsymbol{\Phi}_S \boldsymbol{L}^{\mathsf{T}} (\boldsymbol{Y} - \boldsymbol{L}\boldsymbol{\Phi}_s \boldsymbol{C} \boldsymbol{\Phi}_t^{\mathbb{H}}) \boldsymbol{\Phi}_t$,
Ensure: $\tau = 1$
  while $||\boldsymbol{Z} - \boldsymbol{Z}_0||_F >$ tolerance **do**
    $\boldsymbol{Z}_0 \Leftarrow \boldsymbol{Z}$
    $\boldsymbol{Z} \Leftarrow \text{prox}_{\ell_1 + \ell_{1,2}} (\boldsymbol{C} + \boldsymbol{X})$
    $\tau_0 \Leftarrow \tau$
    $\tau \Leftarrow 1 + \sqrt{1 + 4\tau_0^2}/2$
    $\boldsymbol{C} \Leftarrow \boldsymbol{Z} + \boldsymbol{Z}_0(\tau_0 - 1)/\tau$
  end while

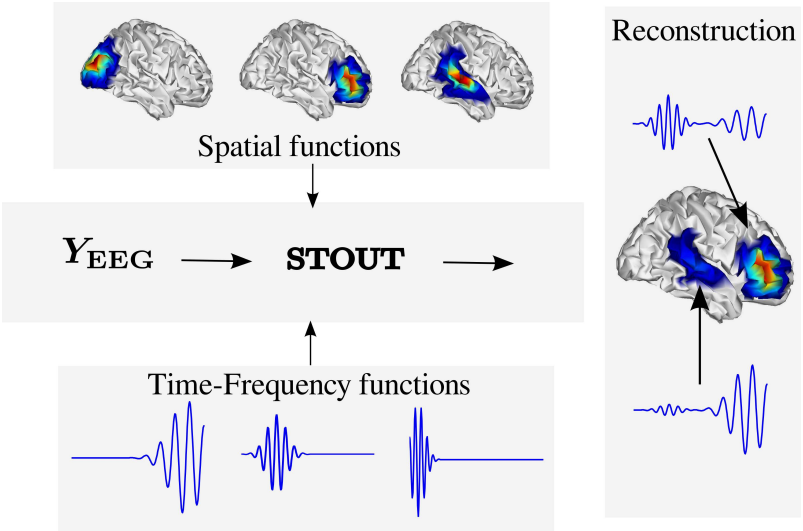

Figure **4-1**.: Illustrative example of STOUT.

space and time–frequency dictionaries. In the first case, given that the ground truth is available for the simulated EEG, we tune the values of both regularization parameters, λ_t and λ_s, in accordance to the proposed residual norm criterion that we define as follows:

$$\gamma = ||\boldsymbol{Y} - \boldsymbol{LJ}||_F^2 / ||\boldsymbol{Y}||_F^2,$$

The regularization parameters are iteratively calculated to get reconstructions with the residual norm closest to the ideal one in each run. Specifically, the regularization parameters are initialized to obtain an all-zero reconstruction for each simulation, then at each iteration the parameters are decreased by a factor of 0.7 until the ideal residual norm is reached. The same procedure is used for the three considered methods S-FLEX, TF-MxNE and STOUT.
About the sparse basis fields needed in Eq. (4-3), they are constructed as follows

- *Spatial dictionary*, $\boldsymbol{\Phi}_s$, is built in the form of Gaussian functions that are placed at every discrete dipole:

  $$\boldsymbol{\Phi}_s(i,j) = \exp\{-d_g\{\boldsymbol{x}_{(i)}, \boldsymbol{x}_{(j)}\}^2 / \sigma^2\},$$

  where $\boldsymbol{\Phi}_s(i,j) \subset \mathbb{R}^+$ is the value of the i-th element of the dictionary at jth dipole, $d_g\{\boldsymbol{x}_{(i)}, \boldsymbol{x}_{(j)}\} \subset \mathbb{R}^+$ is the geodesic distance along the cortical surface between i-th and j-th dipole, $\sigma \subset \mathbb{R}^+$ is the width of every used Gaussian function. The σ is to be selected to get solutions having adequate spatial resolution (i.e., narrow functions), but at the same time, as to promote local smoothness (i.e., wide functions). In the concrete case, this value is heuristically fixed as $\sigma = 1\,cm$.

- *Time-frequency dictionary*, $\boldsymbol{\Phi}_t$, is built using as the basis function the Short Time Fourier Transform (STFT) having frequency resolution of $1.2\,Hz$, time shift length of 10 samples, and using a Gaussian window.

4.4. Results of simulated EEG data

To illustrate the temporal and spatial structure encouraged by STOUT, we carried out a simplified estimation experiment using a randomly generated lead field matrix modeling 20 *virtual* electrodes and 50 *virtual* dipoles. Figure **4-2** shows amplitude and sparsity pattern obtained for several methods. LORETA reconstruction yielded an irrelevant sparsity pattern and a noisy and blurry reconstruction. Furthermore, ℓ_1 norm estimation achieved scattered spatial sparsity, and the temporal structure does not correspond to the simulated activity. On the other hand, S-FLEX achieved well structured spatial patterns due to the spatial basis functions, although, since temporal dynamics are not taken into account, the time-frequency pattern is poorly recovered. Furthermore, TF-MxNE achieves a good temporal pattern although the spatial structure does not correspond to the simulation (scattered sources). Finally, STOUT achieved the best reconstruction: it preserves spatial and temporal patterns of the simulated activity which is encouraged by the space-time-frequency dictionaries.

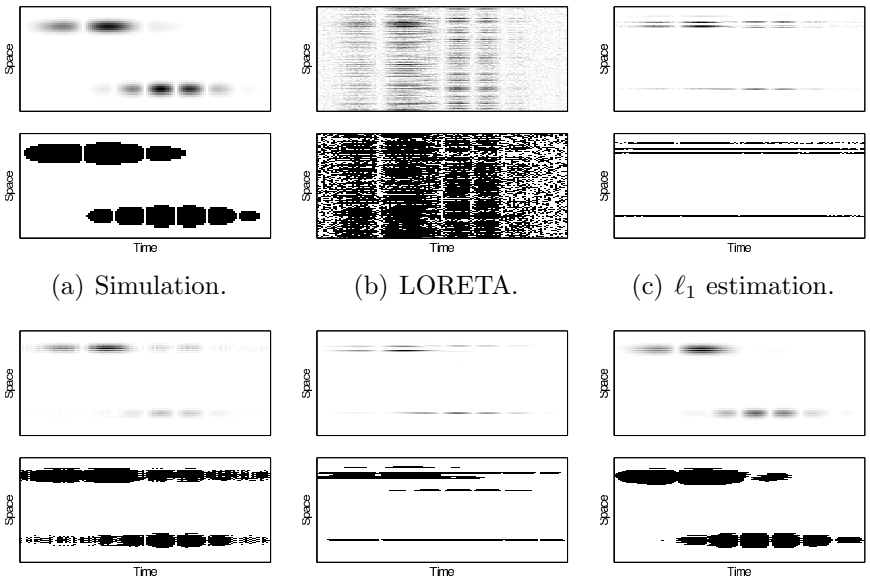

(a) Simulation. (b) LORETA. (c) ℓ_1 estimation.

(d) S-FLEX. (e) TF-MxNE. (f) STOUT.

Figure **4-2**.: Time-space representation of the amplitude and sparsity patterns of reconstruction achieved for several baseline methods and STOUT.

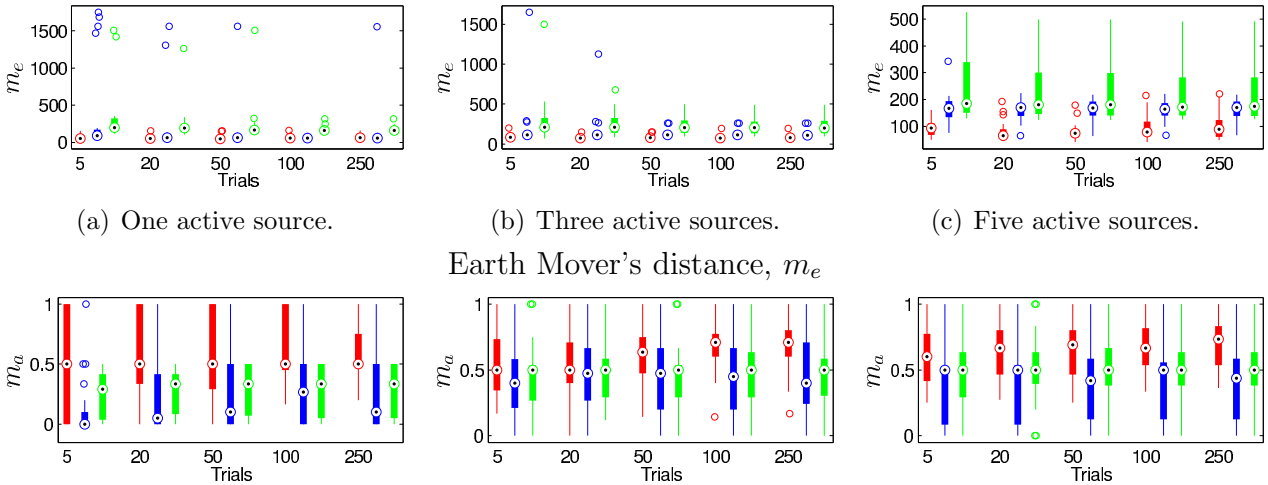

(a) One active source. (b) Three active sources. (c) Five active sources.

Earth Mover's distance, m_e

(d) One active source. (e) Three active sources. (f) Five active sources.

Spatial accuracy index, m_a

Figure **4-3**.: Assessed spatial quality of brain mapping for :
■S-FLEX ■TF-MxNE ■STOUT

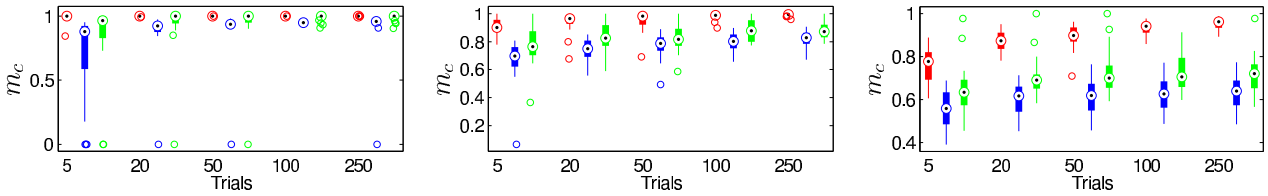

(a) One active source. (b) Three active sources. (c) Five active sources.

Figure **4-4**.: Average of the maximum correlation computed for each estimator.
■S-FLEX ■TF-MxNE ■STOUT

Top row of Figure **4-3** shows m_e computed for each simulation scenario. According to this measure, the method with the best performance is S-FLEX, followed by TF-MxNE and then STOUT. There are not significant changes in the performance of the considered method for different SNR values. Furthermore, besides having the worst performance, STOUT has the highest dispersion, although, in general, its performance is similar to TF-MxNE.
Moreover, bottom row of Figure **4-3** shows m_a computed for simulated data. For a single active source, S-FLEX and STOUT have a clear advantage with respect to TF-MxNE. Furthermore, the dispersion of S-FLEX is highly affected by noise. Furthermore, for three and five active sources, the performance of the three methods are almost equivalent, although S-FLEX has a slight advantage with respect to STOUT and TF-MxNE.
As regards the temporal component of the reconstruction, Figure **4-4** depicts attained m_c. Puzzling, under every considered scenario, S-FLEX has the best performance, followed by STOUT, and then TF-MxNE which has the worst performance according to m_c. For different number of sources, the behavior is the same, although for five active sources, S-FLEX is slightly more sensitive to noise than TF-MxNE and STOUT.

4.5. Real EEG Data

4.5.1. Database

STOUT was tested on real-world data in order to localize neural sources of auditory and visual evoked potentials. In this regard, fifteen healthy subjects participated in an ERP study which was designed to compare the evoked potentials from two sensory modalities in the context of a brain-computer interface. Subjects alternately perceived sequences of either auditory (condition A) or visual (condition V) stimuli. This data was recorded within a different study, which is precisely described in [**?**]. In both conditions A and V, the stimuli had a duration of 130 ms while the time delay between the onsets of two consecutive stimuli was 200 ms.
In each trial, six physically different stimuli were repetitively presented in a balanced and pseudorandom order. This design resulted in a sequence of 36 stimuli per trial. During each trial the subject had the task to allocate attention to a predefined stimulus (target) and to count its occurrences, while neglecting the remaining five stimuli (non-targets). The study was designed such that condition A and V only differed in the type of stimulus presentation such that the ERP responses for the two sensory modalities can be compared for each subject. For condition V, six

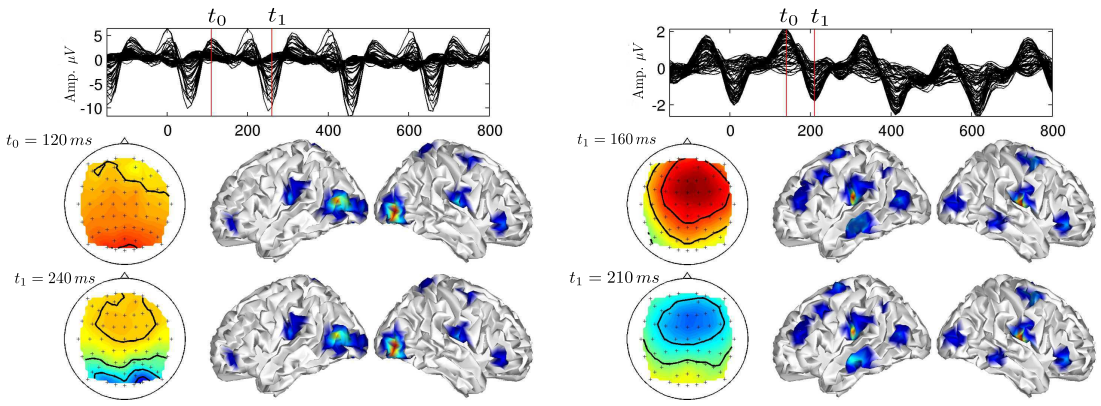

(a) Condition V, Subject 13.

(b) Condition A, Subject 2.

Figure **4-5**.: Non-Target stimuli response of two subjects.

visual stimuli differing in color and shape were presented in the center of a 19" screen. For condition A, six naturally recorded auditory stimuli (i.e. spoken syllables recorded from several voices) differing in pitch and spatial direction were presented on headphones. For each condition, there were 24 trials resulting in a total number of 144 target stimuli and 720 non-target stimuli per subject.

EEG data was recorded with 63 electrodes, symmetrically placed at the standard positions of the international $10-20$ system. For off-line analysis, the EEG data was downsampled to $100\,Hz$, band-pass filtered between 0.4 and $23\,Hz$ and epoched around each stimulus presentation (from $150\,ms$ before stimulus onset to $800\,ms$ after stimulus onset). EEG epochs which contained eye- and muscle artifacts were removed. The Event Related Potential (ERP) for the targets and non-targets were then computed by averaging over the remaining epochs for each condition and subject. STOUT was then applied to find the neuronal sources which generate the ERP.

4.5.2. Results

Figures **4-7**.a and **4-7**.b show two examples of reconstructions achieved for non-target visual and auditory stimuli, respectively. In both cases, STOUT identified the areas associated with presented stimuli, i.e., activation of the area right above the temporal lobe for auditory stimuli and activation of the occipital lobe for visual stimuli.

Furthermore, Figures **4-6** shows the reconstruction provided by STOUT for target auditory and visual stimuli. Similar to non-target stimuli responses shown in Figure **4-7**, the areas corresponding to auditory and visual primary cortices are also activated. However, significant activity appears in the frontal lobes, and may be related to conscious stimuli processing, as expected for target stimuli,

Figures **4-7**.a and **4-7**.b show the average across all subjects of the non-target visual and auditory stimuli reconstruction. Once again, it is shown that STOUT reconstructed activity in the areas associated with the primary visual and auditory cortices. However, for some specific subjects some spurious sources appeared on areas of the brain non-related with the studied phenomenon.

Average reconstructions attained for target visual and auditory stimuli responses are shown in

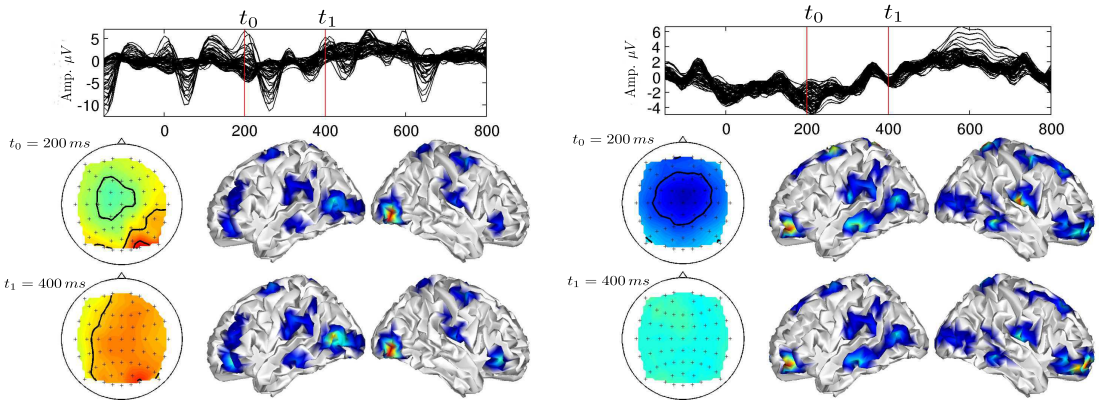

(a) Condition V, Subject 12.

(b) Condition A, Subject 9.

Figure **4-6**.: Example of reconstruction achieved for both conditions, for Target stimuli. The first red vertical line corresponds to the first scalp map and corresponding reconstruction, while the second red vertical line corresponds to the scalp maps and reconstruction shown in the bottom of each subfigure.

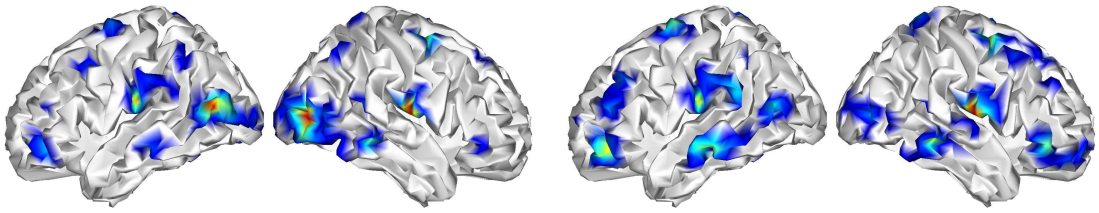

(a) Condition V.

(b) Condition A.

Figure **4-7**.: Average of the reconstruction across all subjects for non-target stimuli, for both conditions.

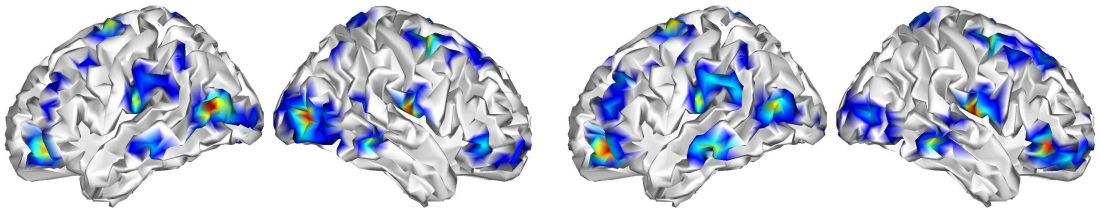

(a) Condition V. (b) Condition A.

Figure **4-8**.: Average of the reconstruction across all subjects for target stimuli, for both conditions.

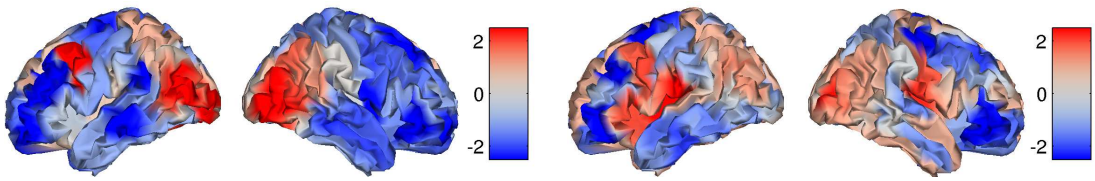

(a) Condition V NT vs Condition A NT (b) Condition V NT vs Condition V T

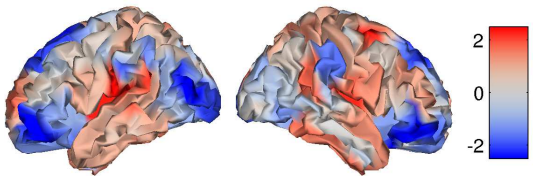

(c) Condition A NT vs Condition A T

Figure **4-9**.: T-test scores to compare the active areas of the brain for both conditions, for Target and Non-target stimuli. NT: NonTarget. T:Target.

Figures **4-8**.a and **4-8**.b, respectively. In this case, the results are not as conclusive as for non-target responses. The averages show activity spread almost all over the cortex. Nevertheless, activity right above the temporal lobe and on the occipital lobe remains for auditory and visual stimuli, respectively. There is also significant activity in the frontal lobes, which, as stated before, is associated with conscious perception and is expected for target stimuli processing.

Figure **4-9**.a shows the t-scores obtained by the t-student test when comparing brain responses to non-target visual vs non-target auditory stimuli. Results show that the first statistical group corresponds to the occipital lobes -associated with visual stimuli responses- while the other group corresponds mainly to part of the primary auditory cortex, although it is also associated with the frontal lobe.

Furthermore, t-scores were also calculated to compare responses obtained for target and non-target stimuli, for both conditions. Figure **4-9**.b shows the results for condition V, here it can be clearly seen that one of the statistical groups are the frontal lobes, however, the occipital lobes (visual cortex) do not have a significant score. On the other hand, Figure **4-9**.c shows the results for auditory stimuli, as for condition V, one of the statistical groups are the frontal lobes (although with some spurious sources in the occipital area), while the other group is the area surrounding the primary auditory cortex.

4.6. Discussion

We introduced STOUT as a method to constraint brain activity estimation in the temporal domain through a set of sparse data-driven temporal dynamics, while keeping spatial coherence. Here, spatial coherence means that activity is found in smooth focal areas. The proposed approach is inspired by two different methods including the features encouraged by STOUT: S-FLEX for spatial consistency and coherence, and TF-MxNE to model temporal dynamics of neural activity using data-driven time-frequency constraints.

In the comparative study carried out to analyze the effects of the considered temporal and spatial constraints in reconstruction quality, S-FLEX, TF-MxNE and STOUT were compared. Although, there was not a significant difference between the performance of the three considered methods, TF-MxNE had to lowest performance, next to STOUT. In general, S-FLEX had the best performance in every considered scenario. Although we did not arrived to a strong conclusion in this regard, this results may be caused by an incorrectly tunning of the regularization parameters (the ratio between spatial and temporal regularization parameters is empirically set), also, the existence of simulated biological noise may hinder the suitability of the residual norm as tunning criterion.

As stated above, one of the most important aspects to consider is the tunning of spatial and temporal constraints used by STOUT. Properties of the spatial domain concerns the construction of the spatial basis functions dictionary; in this regard, a balance should be kept between a dictionary that provides a smooth solution -wide blobs- and a dictionary that allows to reconstruct focal sources -narrow blobs-. In the temporal domain, the parameters are those that control STFT resolution, or more generally speaking, the time frequency structure of the temporal dictionary. The balance between time and frequency resolutions should be carefully analyzed (a standard consideration in any time-frequency analysis), but more importantly, it must be taken into account that the time-frequency representation detail should be fine enough to discriminate close dynamics, but not so fine that it leads to computationally infeasible problems due memory and time resources needed to solve the iterative optimization stage. As a final remark in this regard, the parameters of the dictionary used for reconstructions performed in the present work were empirically balanced.

The experiments for real data provided a deeper insight into the performance and behavior of STOUT. Encouraged spatial coherence allowed to focally identify the generators of the responses to target and non target stimuli. On the other hand, the de-noising effect of encouraged time-frequency sparsity allowed to obtain a good performance for experiments where only a few number of trials were available, namely, responses to target stimuli. This is important since, normally, the number of target stimuli responses available is significantly lower than the number of non-target responses in this type of experiments.

As stated before, the computational cost of STOUT can be problematic if one -or both- dictionaries are big enough. This may a be drawback, since STOUT's precision is limited by computational resources available. To address this issue, as a future work, the use of a data-driven dictionary reduction should be carried out as preprocessing stage to lower the computational cost but without sacrificing reconstruction accuracy.

4.7. Summary

In the present chapter, we have introduced the Spatio-TempOral Unifying Tomography (STOUT), which allows to represent brain activity through a sparse set spatial and time-frequency basis functions, attending to the physiologically motivated assumptions of spatially coherence and complex temporal dynamics. Although, results obtained for simulations suggested that STOUT is not more accurate than the reference methods -S-FLEX and TF-MxNE-, its performance is competent. Besides it is also suitable for real data, specifically reconstruction of ERP. However, some critical issues should be addressed to improve its performance. First, the tunning of the regularization parameters heavily affects the solution, therefore, it is quite probable that the use of heuristically tunned parameters may hinder the performance of STOUT.

5. Conclusions and Future Work

5.1. General Conclusions and Main Contributions

Development of an iterative algorithm to estimate neural activity and its generation model - IRA

In chapter 2, we have developed a novel method to dynamically constrain the time-domain dynamics of brain activity estimation through a realistic non linear time-varying state space model. The use of such model improves the brain mapping accuracy compared to a state of the art method introduced in [3, 10], where a linear static model is used. However, compared to a method where the time-domain dynamics are implicitly modeled (LOR_p), several comments should be made regarding the proposed method: Robustness to noise provided by IRA and potential interpretability of the non linear model parameters also implies a lack of flexibility of the algorithm, i.e., the model used in the state transition equation may not properly describe brain dynamics of a given phenomenon, therefore, IRA requires a considerable analysis overhead to assess the suitability of a given model with respect to the studied phenomenon. Furthermore, the convergence of the model parameters is also a critical and problematic issue, probably because of the large amount of hidden parameters that should be estimated (activity in each dipole and parameters of the model) from the same set of available data, however this should be studied in more depth. From this chapter we have concluded that the automatic identification of brain dynamics -as in LOR_p- is a more feasible approach to include time domain a priori information in the EEG inverse problem than an explicit state space model, nevertheless IRA had a performance at least comparable to the baseline methods.

Design of a Bayesian estimation framework using time-varying a priori information - DOBERMAN

The dynamically constrained framework presented in chapter 3 showed that the assumption of spatial non-stationarity and sparsity, as expected in brain activity, improves the spatial accuracy of brain activity estimation. Furthermore, the analysis carried out for real data showed that the time-varying hyperparameters may provide a deep insight about the underlying neural processes and relations between spatially coherent areas of the brain. Nevertheless, the use of the SVD to identify the main time-domain dynamics is less robust to noise than other approaches -as IRA- and may not be completely suitable to identify the most complex dynamics found in EEG recordings. Therefore, different decomposition models should be studied to provide robustness to noise and also identify more complex dynamics that may be potentially useful for the spatial dictionary used to construct the time-varying a priori covariance matrix.

Design of mapping algorithm representing brain activity through predefined sparse sets of space-time-frequency dictionaries - STOUT

Finally, we have introduced a novel method that allows to represent brain activity through a sparse set of space and time-frequency basis functions, in chapter 4. The contribution -termed STOUT- is inspired by two state of the art approaches, namely S-FLEX and TF-MxNE. Although the assessed performance for simulated scenarios showed that STOUT did not improve brain mapping accuracy, results obtained for real data proved that the proposed method is suitable for reconstructing Evoked Response Potentials, and yields physiologically meaningful solutions: spatially coherent activity and smooth time series. Nevertheless, one of the drawbacks related with STOUT is the tuning of the regularization parameters. Although, the residual norm criterion helps to get close to an *optimal* regularization, the ratio between the spatial and temporal regularization parameters was heuristically tuned. With this approach, STOUT and TF-MxNE (the methods with two regularization terms) may be under-regularized given that the regularization energy is split between two functionals. Finally, the construction of spatial and temporal dictionaries with different structures as the considered in the present study should be also addressed as future work.

5.2. Future Work

Besides the method-specific analyzes proposed above as future work, more general topics should also be taken with special consideration:

Identification of main dynamics in EEG recordings

In general, the automatic identification of time-domain dynamics carried out in this thesis was achieved using the Singular Value Decomposition -in the case of DOBERMAN-, or the Short Time Fourier Transform -in the case of STOUT-. However, there should be a deep analysis regarding different methods to extract the dynamics of the EEG signals, e.g., separation of stationary and non stationary components. Such techniques could provide more accurate solutions under strong non-stationarity conditions or when the studied phenomenon posses complex time-domain dynamics not identifiable by the considered techniques.

Interpretability of the EEG inverse problem solution

Typically, EEG-based brain mapping solutions provide valuable information about active areas of the brain (spatial information). One of the contributions of this work was to analyze how the temporal information provided by EEG signals could be used to improve the inverse solution accuracy. Bearing this in mind, as future work, brain connectivity studies should be carried out using the techniques proposed in this thesis, because the obtained results contain not only spatial information, but also they may provide information about how specific brain areas interact with each other with outstanding temporal resolution.

A. Appendix: Depth compensation analysis

Since it is difficult for EEG recordings to detect deep neural generators, brain mappings are typically biased towards reconstructing superficial sources. Typically, to cope with this issue, a preprocessing stage known as "depth bias compensation" is carried out. The goal is to allow reconstruction of deep sources even when their activation is unlikely.
In the present section we study two options which, in general, represent the available methods to carry out the aforementioned preprocessing stage, and determine which one should be utilized according to the lead field data used in this thesis.

A.1. Depth compensation based on the lead field matrix norm

Usually, the columns of the lead field matrix $\boldsymbol{L}$ may be normalized with respect to their ℓ_2 norm. However, as stated in [11], for the EEG inverse problem this may not be the optimal approach since it tends to over compensate the depth of the sources, i.e., solutions are susceptible of reconstructing the deepest sources even when such sources do not explain measured activity. In [11], it has been proposed to use a similar approach (normalization of the columns of $\boldsymbol{L}$) but with a parameter that allows to control how strong the depth compensation is.
Specifically, for the ith column of $\boldsymbol{L}$, i.e., $\boldsymbol{L}(\cdot, i)$, the normalization term is calculated as follows

$$\Omega(i,i) = \sqrt{(||\boldsymbol{L}_x(\cdot,i)||_2^2 + ||\boldsymbol{L}_y(\cdot,i)||_2^2 + ||\boldsymbol{L}_z(\cdot,i)||_2^2)^{\zeta}} \tag{A-1}$$

where $\Omega \subset \mathbb{R}^{3N_d \times 3N_d}$ is the normalization matrix, and $0 < \zeta < 1$ is a parameter that determines how strong the depth compensation is. When $\zeta = 0$, there is no depth bias compensation, on the other hand, $\zeta = 1$ leads to full compensation. For the present work, it was empirically fixed as $\zeta = 0.6$.

A.2. Depth compensation based on pre-estimated variance

On the other hand, in [13] it has been shown that the depth compensation can be carried out using a pre-estimation of the variance of the sources. Specifically, this compensation method is based on the sLORETA algorithm presented in [21]. In this regard, the estimate variance is computed as $\widehat{\boldsymbol{\Upsilon}} = \boldsymbol{L}^{\mathsf{T}}(\boldsymbol{L}\boldsymbol{L}^{\mathsf{T}})^{-1}\boldsymbol{L}$. Then the depth compensation matrix is defined as

$$\boldsymbol{\Omega} = \begin{pmatrix} \boldsymbol{W}_1 & \dots & 0 \\ \vdots & \ddots & \vdots \\ 0 & \dots & \boldsymbol{W}_{N_d} \end{pmatrix} \tag{A-2}$$

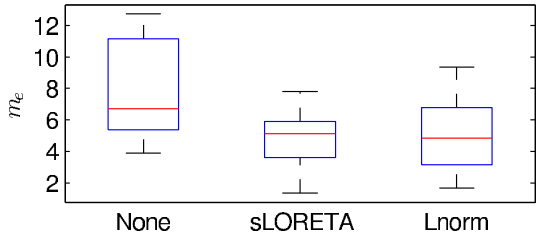

Figure **A-1**.: Earth mover's distance achieved for different depth compensation methods.

where $\boldsymbol{W}_i \subset \mathbb{R}^{3\times 3}$ is the ith block element of $\boldsymbol{\Omega}$ and corresponds to the matrix square root of the ith block element of $\widehat{\boldsymbol{\Upsilon}}$ [14].

A.3. Results

To assess the performance of the two depth compensation methods considered, we simulated a single active source and 100 trials, following the same guidelines described in section 2.3.1 and used as brain mapping method the Sparse Basis Field Expansion (S-FLEX) [14] algorithm.
Figure **A-1** shows the Earth mover's distance obtained for the aforementioned simulations. It can be seen that the inclusion of a depth compensation stage improves the accuracy of the reconstruction. Furthermore, the performance attained with sLORETA-based and $\boldsymbol{L}$-norm based depth compensation does not show significant differences.

A.4. Conclusions

Although the results obtained do not offer enough evidence to state a sound conclusion, for the specific lead field matrix used in the present work, the sLORETA-based depth bias compensation tends to overcompensate depth sources. Given that for our brain model, the source are located only in the cortical manifold, such strong compensation could hinder the performance of any of the considered methods. Consequently, throughout this work, we have decided to use the depth compensation based on the norm of the lead field matrix columns. However, it should be stated that the depth compensation method used in a particular study should be carefully selected depending on the specific brain model used.

B. Appendix: Academic Discussion

This thesis has lead to three works presented in international conferences and one national symposium. Furthermore, two manuscripts have been sent to peer-reviewed journals.

- J.S. Castaño-Candamil, J.D. Martinez-Vargas, C.G. Castellanos-Dominguez. *Dynamically Constrained Mapping of Non-Stationary Brain Activity.* Journal: NeuroImage. 2014. (Under review)

- J.S. Castaño-Candamil, E. Giraldo-Suarez, C.D. Acosta-Medina,C.G. Castellanos-Dominguez. *Neural Activity Estimation from EEG using an Iterative Dynamic Inverse Problem Solution.* Journal Cognitive Computation. 2013. (Under review).

- J.V. Hurtado Rincon, J.S. Castaño-Candamil, C.G. Castellanos-Dominguez. *Inclusion of temporal constraints in the EEG inverse problem: A comparative study*, XVIII Symposium of Image, Signal Processing, and Artificial Vision (STSIVA), 2013

- E. Giraldo-Suarez, J.S. Castaño-Candamil, C.G. Castellanos-Dominguez. *A Weighted Dynamic Inverse Problem for Electroencephalographic Current Density Reconstruction.* 6th International IEEE EMBS Conference on Neural Engineering. 2013.

- J.S. Castaño-Candamil, J.D. Martinez-Vargas, C.G. Castellanos-Dominguez. *Bayesian Estimation of Neural Activity for Nonstationary Sources using Time Frequency-based Priors.* 6th International IEEE EMBS Conference on Neural Engineering. 2013.

Bibliography

[1] Baillet, Sylvain ; Mosher, John C. ; Leahy, Richard M.: Electromagnetic Brain Mapping. En: *Signal Processing Magazine, IEEE* 18 (2001), Nr. November, p. 14 –30

[2] Barton, M.; ; Robinson, P.; ; Kumar, S.; ; Galka, A.; ; Durrant-White, H.; ; Guivant, J. ; Ozaki, T.;: Evaluating the Performance of Kalman-Filter-Based EEG Source Localization. En: *IEEE Transactions on Biomedical Engineering* 56 (2009), January, Nr. 1, p. 435 –453. – ISSN 0018–9294

[3] Barton, Matthew J. ; Robinson, Peter a. ; Kumar, Suresh ; Galka, Andreas ; Durrant-Whyte, Hugh F. ; Guivant, José ; Ozaki, Tohru: Evaluating the performance of Kalman-filter-based EEG source localization. En: *IEEE transactions on bio-medical engineering* 56 (2009), Januar, Nr. 1, p. 122–36. – ISSN 1558–2531

[4] Beck, Amir ; Teboulle, Marc: A Fast Iterative Shrinkage-Thresholding Algorithm for Linear Inverse Problems. En: *SIAM J. Img. Sci.* 2 (2009), März, Nr. 1, p. 183–202. – ISSN 1936–4954

[5] Belardinelli, Paolo ; Ortiz, Erick ; Barnes, Gareth ; Noppeney, Uta ; Preissl, Hubert: Source Reconstruction Accuracy of MEG and EEG Bayesian Inversion Approaches. En: *PloS one* 7 (2012), Dezember, Nr. 12, p. e51985. – ISSN 1932–6203

[6] Connors, WarrenA. ; Trappenberg, Thomas: Improved Path Integration Using a Modified Weight Combination Method. En: *Cognitive Computation* 5 (2013), Nr. 3, p. 295–306. – ISSN 1866–9956

[7] Durka, Piotr J. ; Matysiak, Artur ; Montes, Eduardo M. ; Sosa, Pedro V. ; Blinowska, Katarzyna J.: Multichannel matching pursuit and EEG inverse solutions. En: *Journal of neuroscience methods* 148 (2005), Nr. 1, p. 49–59

[8] Friston, K. J. ; Mattout, J. ; Bareto, Trujillo N. ; Ashburner, J. ; Penny, W. D.: Variational free energy and the Laplace approximation. En: *NeuroImage* 34 (2007), Nr. 1, p. 220–234

[9] Friston, Karl ; Harrison, Lee ; Daunizeau, Jean ; Kiebel, Stefan ; Phillips, Christophe ; Trujillo-Barreto, Nelson ; Henson, Richard ; Flandin, Guillaume ; Mattout, Jérémie: Multiple sparse priors for the M/EEG inverse problem. En: *NeuroImage* 39 (2008), Nr. 3, p. 1104 – 1120. – ISSN 1053–8119

[10] Galka, Andreas ; Yamashita, Okito ; Ozaki, Tohru ; Biscay, Rolando ; Valdés-Sosa, Pedro: A solution to the dynamical inverse problem of EEG generation using spatiotemporal Kalman filtering. En: *NeuroImage* 23 (2004), Oktober, Nr. 2, p. 435–53. – ISSN 1053–8119

[11] Gramfort, A. ; Strohmeier, D. ; Haueisen, J. ; Hämäläinen, M.S. ; Kowalski, M.: Time-frequency mixed-norm estimates: Sparse M/EEG imaging with non-stationary source activations. En: *NeuroImage* 70 (2013), Nr. 0, p. 410 – 422. – ISSN 1053–8119

[12] Grech, Roberta ; Cassar, Tracey ; Muscat, Joseph ; Camilleri, Kenneth ; Fabri, Simon ; Zervakis, Michalis ; Xanthopoulos, Petros ; Sakkalis, Vangelis ; Vanrumste, Bart: Review on solving the inverse problem in EEG source analysis. 5 (2008), june, Nr. 25, p. 792 –800. – ISSN 0018–9294

[13] Haufe, Stefan ; Nikulin, Vadim V. ; Ziehe, Andreas ; Müller, Klaus-Robert ; Nolte, Guido: Combining sparsity and rotational invariance in EEG/MEG source reconstruction. En: *NeuroImage* 42 (2008), Nr. 2, p. 726 – 738. – ISSN 1053–8119

[14] Haufe, Stefan ; Tomioka, Ryota ; Dickhaus, Thorsten ; Sannelli, Claudia ; Blankertz, Benjamin ; Nolte, Guido ; Müller, Klaus-Robert: Large-scale EEG/MEG source localization with spatial flexibility. En: *NeuroImage* 54 (2011), Nr. 2, p. 851 – 859. – ISSN 1053–8119

[15] Hillebrand, Arjan ; Barnes, Gareth: The use of anatomical constraints with MEG beamformers. En: *NeuroImage* 20 (2003), Dezember, Nr. 4, p. 2302–2313. – ISSN 10538119

[16] Hoehne, Johannes ; Schreuder, Martijn ; Blankertz, Benjamin ; Tangermann, Michael: A novel 9-class auditory ERP paradigm driving a predictive text entry system. En: *Frontiers in Neuroscience* 5 (2011), Nr. 99. – ISSN 1662–453X

[17] Kim, J. ; Robinson, P.: Compact dynamical model of brain activity. En: *Physical Review E* 75 (2007), März, Nr. 3, p. 031907. – ISSN 1539–3755

[18] Kim, J. W. ; Shin, H.-B. ; Robinson, P. A.: Compact continuum brain model for human electroencephalogram. En: *Society of Photo-Optical Instrumentation Engineers (SPIE) Conference Series* Vol. 6802, 2007

[19] Michel, Christoph M. ; Murray, Micah M. ; Lantz, Göran ; Gonzalez, Sara ; Spinelli, Laurent ; Grave de Peralta, Rolando: EEG source imaging. En: *Clinical neurophysiology : official journal of the International Federation of Clinical Neurophysiology* 115 (2004), Oktober, Nr. 10, p. 2195–222. – ISSN 1388–2457

[20] Miwakeichi, Fumikazu ; Martinez-Montes, Eduardo ; Valdés-Sosa, Pedro A. ; Nishiyama, Nobuaki ; Mizuhara, Hiroaki ; Yamaguchi, Yoko: Decomposing {EEG} data into space–time–frequency components using Parallel Factor Analysis. En: *NeuroImage* 22 (2004), Nr. 3, p. 1035 – 1045. – ISSN 1053–8119

[21] Pascual-Marqui, R D.: Standardized low-resolution brain electromagnetic tomography (sLORETA): technical details. En: *Methods and findings in experimental and clinical pharmacology* 24 Suppl D (2002), p. 5–12. – ISSN 0379–0355

[22] Pascual-Marqui, Roberto ; Michel, Christoph M. ; Lehman, Dietrich: Low Resolution Electromagnetic Tomography: A New Method for Localizing Electrical Activity in the Brain. En: *International Journal of Psychophysiology* (1994), Nr. 18, p. 49–65

[23] Pascual-marqui, Roberto D.: Review of Methods for Solving the EEG Inverse Problem. En: *International Journal of Bioelectromagnetism* 1 (1999), Nr. 1, p. 75–86

[24] Phillips, Christophe ; Rugg, Michael D. ; Friston, Karl J.: Anatomically Informed Basis Functions for {EEG} Source Localization: Combining Functional and Anatomical Constraints. En: *NeuroImage* 16 (2002), Nr. 3, Part A, p. 678 – 695. – ISSN 1053–8119

[25] Phillips, Christophe ; Rugg, Michael D. ; Friston, Karl J.: Systematic Regularization of Linear Inverse Solutions of the {EEG} Source Localization Problem. En: *NeuroImage* 17 (2002), Nr. 1, p. 287 – 301. – ISSN 1053–8119

[26] Plummer, C.; ; Simon-Harvey, A. ; Cook, M.;: EEG source localization in focal epilepsy: Where are we now? En: *Epilepsy* 49 (2008), june, Nr. 2, p. 201 –218. – ISSN 0018–9294

[27] Schmitt, U ; Louis, a K.: Efficient algorithms for the regularization of dynamic inverse problems: I. Theory. En: *Inverse Problems* 18 (2002), Juni, Nr. 3, p. 645–658. – ISSN 02665611

[28] Schmitt, U ; Louis, a K. ; Wolters, C ; Vauhkonen, M: Efficient algorithms for the regularization of dynamic inverse problems: II. Applications. En: *Inverse Problems* 18 (2002), Juni, Nr. 3, p. 659–676. – ISSN 02665611

[29] Tibshirani, Robert: Regression Shrinkage and Selection Via the Lasso. En: *Journal of the Royal Statistical Society, Series B* Vol. 58, 1994, p. 267–288

[30] Toga, Arthur ; Mazziotta, John: *Brain Mapping: The Methods*. 2nd. Elsevier Science, 2002. – ISBN 0126930198

[31] Trujillo-Barreto, Nelson J. ; Aubert-Vázquez, Eduardo ; Penny, William D.: Bayesian M/EEG source reconstruction with spatio-temporal priors. En: *NeuroImage* 39 (2008), Januar, Nr. 1, p. 318–35. – ISSN 1053–8119

[32] Van Veen, B D. ; van Drongelen, W ; Yuchtman, M ; Suzuki, a: Localization of brain electrical activity via linearly constrained minimum variance spatial filtering. En: *IEEE transactions on bio-medical engineering* 44 (1997), September, Nr. 9, p. 867–80. – ISSN 0018–9294

[33] Wipf, David ; Nagarajan, Srikantan: A unified Bayesian framework for MEG/EEG source imaging. En: *NeuroImage* 44 (2009), Nr. 3, p. 947 – 966. – ISSN 1053–8119

[34] Yamashita, Okito ; Galka, Andreas ; Ozaki, Tohru ; Biscay, Rolando ; Valdes-Sosa, Pedro: Recursive penalized least squares solution for dynamical inverse problems of EEG generation. En: *Human brain mapping* 21 (2004), April, Nr. 4, p. 221–35. – ISSN 1065–9471

[35] Zwolinski, Piotr ; Roszkowski, Marcin ; Zygierewicz, Jaroslaw ; Haufe, Stefan ; Nolte, Guido ; Durka, Piotr J.: Open Database of Epileptic EEG with MRI and Postoperational Assessment of Foci - a Real World Verification for the EEG Inverse Solutions. En: *Neuroinformatics* 8 (2010), Nr. 4, p. 285–299